# Loss of consciousness is related to hyper-1 correlated gamma-band activity in anesthetized macaques and sleeping humans

Article (Accepted Version)

# Loss of consciousness is related to hyper-correlated gamma-band activity in anesthetized macaques and sleeping humans

**Michał Bola[1], Adam B Barrett[2], Andrea Pigorini[3], Lino Nobili[4], Anil K. Seth[2], Artur Marchewka[1]**

1: Laboratory of Brain Imaging, Neurobiology Center, Nencki Institute of Experimental Biology of Polish Academy of Sciences, Warsaw, Poland

2: Sackler Centre for Consciousness Science, Department of Informatics, University of Sussex, Brighton BN1 9QJ, UK

3: Department of Clinical Sciences, University of Milan, Milan 20157, Italy

4: Centre of Epilepsy Surgery "C. Munari", Niguarda Hospital, Milan, 20162, Italy

**Corresponding author:**
Michał Bola, PhD
Laboratory of Brain Imaging, Neurobiology Center
Nencki Institute of Experimental Biology
Polish Academy of Sciences
3 Pasteura Str., 02-093 Warsaw, Poland
Email: m.bola@nencki.gov.pl

**Abbreviated title**: Hyper-correlated brain activity during loss of consciousness

**Keywords:** Consciousness, anesthesia, sleep, gamma-band, ECoG.

**Acknowledgments:** MB was supported by IBRO InEurope fellowship, START stipend from the Foundation for Polish Science, and Sonata grant from the National Science Centre Poland (2015/17/D/HS6/00269). ABB is funded by EPSRC grant EP/L005131/1. AP was supported by "Sinergia" grant (CRSII3_160803/1) from the Swiss National Science Foundation. The Sackler Centre for Consciousness Science (ABB, AKS) is supported by the Dr. Mortimer and Theresa Sackler Foundation.

**Conflict of interest:** The authors declare no competing interests.

**Author Contributions:** MB: conception and design, analysis and interpretation of data, drafting and revising the article; AB: advising on analysis and statistical methods, interpretation of data, revising the manuscript; AP: sleep data recording and processing, revising the manuscript; LN: supervision of sleep data recording, revising the manuscript; AKS: advising on analysis and statistical methods, interpretation of data, revising the manuscript; AM: supervising analysis, interpretation of data, revising the manuscript

## Abstract

Loss of consciousness can result from a wide range of causes, including natural sleep and pharmacologically induced anesthesia. Important insights might thus come from identifying neuronal mechanisms of loss and re-emergence of consciousness independent of a specific manipulation. Therefore, to seek neuronal signatures of loss of consciousness common to sleep and anesthesia we analyzed spontaneous electrophysiological activity recorded in two experiments. First, electrocorticography (ECoG) acquired from 4 macaque monkeys anesthetized with different anesthetic agents (ketamine, medetomidine, propofol) and, second, stereo-electroencephalography (sEEG) from 10 epilepsy patients in different wake-sleep stages (wakefulness, NREM, REM). Specifically, we investigated co-activation patterns among brain areas, defined as correlations between local amplitudes of gamma-band activity. We found that resting wakefulness was associated with intermediate levels of gamma-band coupling, indicating neither complete dependence, nor full independence among brain regions. In contrast, loss of consciousness during NREM sleep and propofol anesthesia was associated with excessively correlated brain activity, as indicated by a robust increase of number and strength of positive correlations. However, such excessively correlated brain signals were not observed during REM sleep, and were present only to a limited extent during ketamine anesthesia. This might be related to the fact that, despite suppression of behavioral responsiveness, REM sleep and ketamine anesthesia often involve presence of dream-like conscious experiences. We conclude that hyper-correlated gamma-band activity might be a signature of loss of consciousness common across various manipulations and independent of behavioral responsiveness.


## Introduction

Loss of consciousness (LOC) can result from natural sleep-wake cycle, impact of various pharmacological agents, or traumatic brain injury (for reviews see Lydic and Baghdoyan, 2005; Brown et al., 2010). Dreamless sleep, general anaesthesia, and unresponsive wakefulness (vegetative) states differ in many respects, but what they have in common is the absence of subjective conscious experience. Even when considering general anaesthesia alone, consciousness can be suppressed by a range of anaesthetic agents characterised by different pharmacological mechanisms of action (Solt and Forman, 2007; Franks, 2008). Therefore, validating postulated neuronal correlates of loss and re-emergence of consciousness across a variety of distinct experimental manipulations might constitute a crucial test for theories of consciousness.

The Global Neuronal Workspace theory proposes that long-distance communication and information sharing among brain areas are critical for emergence of consciousness (Baars, 2005;

Dehaene and Changeux, 2011). This prediction has been supported by studies showing a decrease in functional and effective connectivity, particularly feedback connectivity from frontal to parietal regions, during general anesthesia (Ku et al., 2011; Lee et al., 2013; Boly et al., 2012) and in unresponsive wakefulness syndrome patients (Boly et al., 2011; King et al., 2013). A different but equally influential theory, Integrated Information Theory, predicts that level of consciousness is associated with the complexity of brain activity (Tononi, 2004; Tononi et al., 2016), where 'complexity' has been defined in a variety of ways (see e.g., Seth et al, 2011). A particularly influential series of studies probed complexity of brain activation patterns evoked by a transcranial magnetic stimulation (TMS). Highly complex activations were indeed observed during wakefulness, but not during NREM sleep, general anesthesia, or in patients with disorders of consciousness (Massimini et al., 2005, 2010; Casali et al., 2013; Sarasso et al., 2015; Pigorini et al., 2015). Importantly, further studies revealed that also spontaneous neurophysiological activity is less complex and dynamic during NREM sleep (Schartner et al., 2016) and general anesthesia (Sara and Pistoia, 2010; Alonso et al., 2014; Schartner et al., 2015; Solovey et al., 2015; Tajima et al., 2015; Wang et al., 2017; Krzemiński et al., 2017).

In the present study, we aimed to test whether patterns of spontaneous co-activations among brain regions constitute manipulation-independent correlates of LOC. Specifically, based on the assumption that gamma-band oscillations are closely related to neuronal firing (Whittingstall and Logothetis, 2009; Le Van Quyen et al., 2016), co-activations were estimated by correlating amplitude of gamma-band activity among electrodes. Based on previous theoretical proposals associating consciousness with 'complex' brain dynamics (Tononi and Edelman, 2008; Chialvo, 2010; Seth et al., 2011), during conscious states we hypothesized to observe intermediate levels of coupling (neither complete dependence, nor full independence) and a balance between positive and negative correlations. Conversely, we expected to observe a departure from such a balanced state during LOC. To test these hypotheses we analyzed electrophysiological data from two independent experiments, recorded from two species (macaques, humans) and involving different manipulations of conscious level (anesthesia, sleep).

## Results

### Anesthesia experiment

We analyzed ECoG recordings from an anesthesia experiment obtained from the open-access Neurotycho database (Nagasaka et al., 2011). In the original study ECoG signals were acquired from 4 macaque monkeys using arrays of 128 electrodes covering the lateral part of the left hemisphere. Altogether 22 experimental sessions were conducted with 4 different anesthetic agents

used across sessions (ketamine, KT; medetomidine, MD; ketamine and medetomidine, KTMD; or propofol, PF; see **Table 1** for details). From each session we selected resting-state eyes-closed ECoG data recorded in three conditions/states: (i) awake before the anesthetic injection (PRE), (ii) during anesthesia-induced unresponsiveness (ANES), (iii) and awake after return of responsiveness (POST). The analysis pipeline is schematically presented in **Fig. 1A**. The temporal evolution of gamma-band *coupling strength*, which was chosen as a primary study measure and defined as an average over all pairwise correlation coefficient values, across two representative experimental sessions is shown in **Fig. 2**.

Initially all experimental sessions were pooled and group-level statistics were calculated. We tested distribution of each measure with the Kolmogorov-Smirnoff test and used either repeated-measures ANOVA if a measure conformed to a Gaussian distribution in all conditions, or non-parametric Friedman test otherwise. When significant effect of a state was found pairwise post-hoc comparisons were conducted between conditions using either parametric paired-samples t-tests or non-parametric Wilcoxon tests. Post-hoc tests were corrected for a number of comparisons (3 in the anesthesia data-set, 6 in the sleep data-set) using the Bonferroni-Holm procedure (Holm, 1979). Considering a repeated-measures design we calculated a standardized difference score ($d_z$) as an indicator of the effect size (Cohen, 1988).

We obtained the mean amplitude (power) of gamma activity (30-45Hz) by averaging the envelopes over time and channels. Gamma-band power was affected by a state ($\chi^2$=16.1, p<0.001), specifically it was higher during POST than during both PRE (Z=3.94, p<0.001, $d_z$=2.04) and ANES (Z=2.48, p<0.025, $d_z$=0.86; **Fig. 3**). Next, we focused on co-activations and found significant effect of a *coupling strength* ($\chi^2$=23.2, p<0.001), namely *coupling strength* was greater during ANES than during PRE (Z=4.1, p<0.001, $d_z$=2.23) and POST (Z=3.63, p<0.001, $d_z$=1.68), but there was no difference between PRE and POST (Z=0.29, p<0.76, $d_z$=0.37). To further corroborate this finding we analyzed $density_+$ and $density_-$, which were defined as the proportion of, respectively, positive or negative statistically significant pair-wise correlations out of all possible correlations. We found a significant effect of a state on d$ensity_+$ ($\chi^2$=23, p<0.001). Post-hoc comparisons revealed that ANES was accompanied by an increase in the number of positive correlations (higher $density_+$) when compared to both PRE (Z=4.1, p<0.001, $d_z$=2.1) and POST (Z=3.5, p<0.001, $d_z$=1.6). At the same time the proportion of significant gamma-band anti-correlations (estimated with respect to the significant positive correlations, i.e. $density_-/density_+$) also exhibited an effect of a state ($\chi^2$=28, p<0.001) and was lower during ANES than during PRE (Z=4.1, p<0.001, $d_z$=1.9) and during POST (Z=3.9, p<0.001, $d_z$=2.0; **Fig. 3D**). Thus, all the used measures indicate that gamma-band activity becomes excessively positively correlated (i.e. hyper-correlated) during general anesthesia (see also **Fig. S2-S3**; additional control analyses: **Fig. S6;** other frequency bands:

**Fig. S7, S8**).

**Anesthetics-specific effects**

All general anesthetics suppress perception and behavioral responsiveness, but they vary in terms of pharmacological mechanisms of action and effects on subjective consciousness (Franks, 2008). Specifically, while propofol typically results in complete loss of consciousness, during ketamine anesthesia subjective internally generated conscious experience is often preserved (Garfield et al., 1972; Collier, 1972; Sarasso et al., 2015). Therefore, we next investigated anesthetics-specific effects on brain activity and co-activations (**Fig. 4**). We did not observe such effects when investigating gamma-band power, as changes in gamma power were grouped around zero for all anesthetics. However, the increase in *coupling strength* was most pronounced during propofol anesthesia. Anesthesia induced by ketamine+medetomidine, medetomidine, or ketamine had weaker effect on gamma-band co-activation patterns. A similar effect, namely greatest shift towards positively correlated brain activity after propofol, was found when analyzing $density_+$ and $density_-$.

We next investigated the topographic patterns of anesthesia-induced changes in gamma-band coupling. Motivated by the postulated importance of high-order associative brain regions for conscious processing (Dehaene and Changeux, 2011; MacDonald et al., 2015; Koch et al., 2016) we hypothesized to observe an increase of gamma-band *coupling strength* at frontal brain regions during propofol anesthesia, but no such effect during ketamine anesthesia. Inspecting the topographical maps we first noticed that ketamine-medetomidine, ketamine, and propofol all caused greatest increase of *coupling strength* in occipital regions, and weakest increases in frontal brain areas (**Fig. 5; Fig. S3, S4**). To establish this effect quantitatively we took advantage of the fact that *coupling strength* was calculated in a time-resolved manner (i.e. within 5s-long time-windows) and conducted between-conditions comparisons within each session and module. Specifically, *coupling strength* from an ANES condition was compared to a median value from a PRE condition using a Wilcoxon test. We confirmed that during ANES occipital and parieto-motor modules exhibited significant increases over baseline in all experimental sessions ($p<0.05$, Bonferroni corrected). Importantly, increases in the frontal module were significant in all ketamine-medetomidine, medetomidine, and propofol sessions, but in only 1 (out of 4) ketamine session.

Finally, in order to quantitatively demonstrate that each anesthetic has an individual spatial signature we used an agglomerative hierarchical clustering algorithm to assess similarity, across sessions of the same monkey, of the topographical maps representing changes in *coupling strength*. Indeed, topographies of changes induced by the same anesthetic agent were estimated as more similar to each other than to maps representing changes induced by other anesthetics (**Fig. 5C**).

Overall, we revealed anesthetics-specific signatures present in the spatial patterns of changes in

gamma-band amplitude coupling. When taking into account the differential effects propofol and ketamine might have on consciousness (Sarasso et al., 2015) our findings suggest that hyper-correlated gamma-band activity occurring at the frontal brain regions might be a mechanism suppressing consciousness. Importantly, the spatial patterns of increase in gamma-band *coupling strength* are unlikely explained by the spatial changes in gamma-band power (**Fig. S5**). Thus, gamma-band amplitude coupling might provide reliable and unique information about conscious level.

**Sleep experiment**

Next we aimed to test whether hyper-correlated gamma-band activity can be observed as a correlate of LOC induced by NREM sleep. We thus analyzed an independent data-set recorded from 10 epilepsy patients implanted for diagnostic purposes with invasive intracerebral electrodes. Four different conditions were identified by an experienced clinician based on polysomnography: i) resting wakefulness (WAKE), ii) REM sleep, iii) the first stable N-REM sleep episode of the night (NREM1); iv) and the final stable NREM sleep episode of the night (NREM2). The two former conditions (WAKE and REM) were considered "conscious" conditions, as patients were aware of their environment during wakefulness and were likely dreaming during REM sleep, whereas the two latter conditions (NREM1 and NREM2) were considered LOC states (Siclari et al., 2013). For each condition around 10 minutes of artefact-free recordings were chosen and the same analysis pipeline was applied as to the macaque ECoG data.

In the sleep data-set gamma-band power exhibited significant effect of a state ($\chi^2$=10, p=0.017) but none of the post-hoc comparisons reached Bonferroni-Holm corrected significance level (**Fig. 6**). However, in agreement with the anesthesia data analysis, we did find reliable differences between conscious and unconscious states when comparing magnitude of gamma-band co-activations. Specifically, *coupling strength* ($\chi^2$=21.4, p<0.001) increases during NREM1 in comparison to both WAKE (p=0.011, $d_z$=1.09) and REM (p=0.011, $d_z$=1.46), and during NREM2 in comparison to both WAKE (p=0.015, $d_z$=1.41) and REM (p=0.017, $d_z$=1.25). Importantly, we did not find a difference between conscious conditions (WAKE vs. REM; p=0.92, d=0.38). Further analyses revealed that $density_+$ ($\chi^2$=22, p<0.001) was higher during NREM1 than WAKE (p=0.011, $d_z$=1.4) and REM (p=0.011, $d_z$=2), whereas NREM2 differed from WAKE (p=0.015, $d_z$=1.43), but not from REM (p=0.18, $d_z$=0.73). Finally, we found a decrease in proportion of anti-correlations ($\chi^2$=17.2, p<0.001) during NREM1, when compared to both WAKE (p=0.01, $d_z$=2.42) and REM (p=0.019, $d_z$=2.55), but NREM2 was not different from WAKE (p=0.054, $d_z$=1.67) or REM (p=0.25, $d_z$=1.07). The spatial distribution of electrodes and the magnitude of changes in gamma

band *coupling strength* are shown in **Fig. 7**. Overall, our analyses indicate that also during sleep hyper-correlated gamma-band activity might constitute a reliable marker of consciousness.

### Discriminative power of gamma-amplitude correlations

In order to test the ability of gamma-band co-activations to discriminate between states we estimated the Receiver Operating Characteristic (ROC) curves for both anesthesia and sleep data-sets (**Fig. 8**). ROC curves were calculated at the group level (by using variance across subjects), and also at the single subject level (by taking advantage of time-resolved analysis and using within-condition variability across time). Area under the ROC curve (AUC) was then estimated to indicate the discriminative power of gamma-band *coupling strength*. AUC=0.5 indicates that a given measure cannot discriminate two conditions above chance level, whereas AUC=0 or 1 means that a threshold exists which divides all data-points correctly into two classes/conditions (i.e. allows perfect classification). Typically, measures characterized by AUC<0.25 or >0.75 are considered to have good discriminative power (Hanley and McNeil, 1982).

In the anesthesia dataset we found that for many sessions the comparison between anesthesia and wakefulness exhibited AUC approaching 1, especially when propofol, medetomidine, and ketamine+medetomidine were used (**Fig. 8A**). This is in agreement with robust anesthesia-induced changes observed on the level of individual sessions (see: **Fig. 2**) Conversely, comparisons between two conscious states (PRE vs. POST) yielded generally lower and more variable values. Further, in the sleep dataset comparisons between conscious (WAKE, REM) and unconscious (NREM1) states on the level of individual subjects resulted in AUC values clustered around 0.75, which still indicates good discriminability (**Fig. 8B**). At the group level AUC for comparisons between conscious and unconscious conditions was greater than 0.75 in both datasets. Therefore, measuring gamma-band amplitude correlations in the resting-state allows reliable discrimination of conscious and unconscious states. Importantly, such discrimination level is achieved not only at the group level, but also at the level of individual subjects using very short (5 s) data segments.

## Discussion

Loss of consciousness (LOC) can result from a wide range of causes, including natural sleep, general anesthesia, or traumatic brain injury. Whereas at the micro-scale level of neuronal circuits mechanisms of sleep and anesthesia are clearly different, both states result in a similar endpoint of unresponsiveness and LOC (review: Lydic and Baghdoyan, 2005; Brown et al., 2010). The main contribution of our work is identifying the same macro-scale correlate of LOC in spontaneous electrophysiological activity recorded from two different species and across two different

manipulations of conscious level. Specifically, we found that gamma-band activity becomes hyper-correlated globally across cortex during propofol anesthesia and NREM sleep. However, hyper-correlated gamma-band activity was not found during REM sleep, and during ketamine anesthesia it was present only to a limited and spatially restricted extent (i.e. in the posterior brain regions). To interpret this finding we refer to a possible dissociation between consciousness and behavioral responsiveness. Specifically we assume that REM sleep and ketamine anesthesia might represent unresponsive but conscious states.

**Consciousness, perception, and responsiveness – a possible dissociation**

The "stream of consciousness" we experience is an internal and purely subjective phenomenon (James, 1890). Therefore, we can only infer that others are enjoying a stream of consciousness based on their ability to process sensory stimuli (perception) and to respond in a goal-directed way (behavioral responsiveness; Teasdale and Jennett, 1974). Identifying overt behavioral responsiveness with consciousness is in agreement with common intuitions and is a gold standard in research and clinical contexts. But it has been suggested that in many instances perception, responsiveness, and consciousness might be in fact dissociated (see **Fig. 1B;** Sanders et al., 2012; Fernandez-Espejo and Owen, 2013; Kouider and Dehaene, 2007). Firstly, during rapid eye movement (REM) sleep we are able neither to perceive our environment nor to control our behavior, but we often experience vivid dreams, which in many (though by no means all) respects are phenomenally similar to waking consciousness (Siclari et al., 2013; review: Nir and Tononi, 2010). Studies using a "serial awakening paradigm" revealed that about 70-80% of awakenings during REM sleep, but only 30-40% of NREM awakenings, were followed by a recall of conscious experience (Siclari et al., 2013, 2017). Secondly, ketamine anesthesia results in behavioral unresponsiveness often accompanied by rich hallucinations, which are unconstrained by the external environment (Garfield et al., 1972; Collier, 1972; Sarasso et al., 2015). That dissociating neuronal correlates of consciousness from correlates of responsiveness is feasible has been demonstrated by TMS-EEG studies, which found low complexity of brain responses during unconscious states (NREM sleep, propofol or xenon aesthesia), but relatively high complexity during unresponsive but presumably conscious states (REM sleep, ketamine anesthesia; Casali et al., 2013; Sarasso et al., 2015). Our finding of gamma-band hyper-correlations during propofol anesthesia and NREM sleep, but not during ketamine anesthesia and REM sleep, is in line with these previous findings. Therefore, we hypothesize that gamma-band amplitude-coupling estimated from spontaneous brain activity might constitute a correlate of consciousness independent of perception or behavioral responsiveness.

Another hypothesis which can be formulated based on our results states that regional increase in gamma-band amplitude-coupling is related to local disruption of information processing in a given brain region. This is suggested when comparing the postulated effects of each anesthetic in terms of perception and consciousness with the spatial patterns of changes in gamma-band *coupling strength* (**Fig. 5**). Specifically, ketamine resulted in a marked increase of coupling at the occipital (sensory) brain regions, which is in line with a postulated loss of perception and responsiveness (i.e. disconnection), but no changes in the frontal (associative) regions, in agreement with maintained conscious experience during ketamine anesthesia (Garfield et al., 1972; Sarasso et al., 2015). Conversely, propofol resulted in pronounced increases in *coupling strength* within both occipital and frontal regions, which might reflect suppression of both perception and consciousness. Thus, we propose that relative independence among frontal brain activations (i.e. absence of gamma-band hyper-correlations) might be necessary in order to support conscious experiences, irrespective of behavioral responsiveness.

However, limitations of our work in terms of associating gamma-band correlations with consciousness are: i) lack of behavioral data from continuous assessment of responsiveness and ii) lack of retrospective subjective reports gathered after recovery from anesthesia and sleep (see: Sarasso et al., 2015; Nieminen et al., 2016; Siclari et al., 2017). Further, previous human studies in which subjects reported experiencing dream-like hallucinations used lower doses of ketamine (1.6 mg/kg in Garfield et al., 1972; 2 mg/kg in Sarasso et al., 2015), whereas doses used here were relatively high (4.3 and 5.9 mg/kg; see **Table 1**). Yet, irrespective of the presence (or not) of conscious experiences, our analysis points towards differential effects of anesthetic agents on macro-scale brain activity. It also allows formulating clear hypotheses for future studies, which can test the role of gamma-band amplitude-coupling in healthy subjects (from whom subjective reports will be acquired retrospectively after recovery from sleep or anesthesia) and in patients diagnosed with disorders of consciousness (who despite persistent behavioral unresponsiveness might actually be able to perceive their environment and have conscious experiences; Owen et al., 2006; Coleman et al., 2007; Bekinschtein et al., 2009; Monti et al., 2010; Cruse et al., 2011; Naci et al., 2014).

**Neurophysiological correlates of LOC**

Whereas neurophysiological activity recorded during anesthesia has been thoroughly investigated in terms of spectral content, recent studies have focused on characterizing neuronal complexity, temporal dynamics, and effective interactions. A rationale behind this line of work is testing directly neuronal mechanisms hypothesized to give rise to conscious experiences (Seth et al., 2009; Tononi et al., 2016) and consequently providing more explanatorily powerful correlates of

consciousness. A now well-established finding is that complexity of electrophysiological signals (both spontaneous and event-related) decrease during unconscious states (Casali et al., 2013; Alonso et al., 2014; Schartner et al., 2015, 2016; Solovey et al., 2015; Tajima et al., 2015; Wang et al., 2017; Krzemiński et al., 2017). Therefore, the excessive inter-dependence of gamma-band activity during LOC fits well with these previous results as it might reflect suppression of information transfer and departure from a critical regime (Chialvo, 2010). In comparison to previous studies, the primary novel aspects of our work are: (i) a focus on gamma-band activity, rather than on broadband signals which entail a strong contribution of low frequencies; (ii) analysis of co-activations (or amplitude-coupling), rather than measures relying mainly on signals phases; (iii) and a straightforward analysis pipeline, in contrast to more complex methods based on auto-regressive models (Solovey et al., 2015) or state-space embedding (Tajima et al., 2015). Of note, our finding of hyper-correlated gamma band activity during NREM sleep in humans is in line with an earlier result of Popa et al. (2009), who found an increase in correlations of gamma-band amplitudes during NREM sleep in cats. Future studies might provide a link between these different lines of work by investigating how identified alterations in amplitude-coupling, which is a hypothesized mechanism modulating activity of neuronal populations (Engel et al., 2013), are related to changes in effective connectivity and complexity of neuronal signals.

Our analyses did not reveal any systematic differences between conscious and unconscious states in terms of gamma-band power. Indeed, comparison of topographic maps indicates that increases in amplitude coupling are unlikely to be explained by changes in power (see: **Fig. S5**), suggesting it is not amplitude itself, but rather how neuronal activity is coordinated across brain regions, that is important in distinguishing conscious states. Considering that gamma activity closely tracks neuronal firing (Whittingstall and Logothetis, 2009; Le Van Quyen et al., 2016), hyper-correlated gamma-band might be a macro-scale reflection of a "bursty" activity pattern observed during sleep and anesthesia (Nir et al., 2011; Lewis et al., 2012; Vizuete et al., 2014; Akeju et al., 2016), as simultaneous bursts occurring at multiple brain locations might cause strong positive correlations. Further, the frontal gamma-band hyper-correlations observed during propofol (but also medetomidine) anesthesia bears some resemblance to the previously reported "alpha anteriorization" effect, i.e. an increase of alpha band power and coherence over frontal regions observed during propofol (Supp et al., 2011; Purdon et al., 2013; Chennu et al., 2016) but not during ketamine anesthesia (Blain-Moraes et al., 2014). Yet, there are also marked differences between these two effects, as "alpha anteriorization" involves simultaneous decrease of alpha power over posterior regions, whereas gamma hyper-correlations were actually most pronounced over posterior areas (during both ketamine and propofol anesthesia). Of note, ketamine and propofol were shown to result in different spectral changes in human EEG – ketamine increases gamma-band

activity (but reduces alpha-band), whereas propofol reduces gamma-band activity (but increases alpha; Lee et al., 2013; Blain-Morales et al., 2014). However, our basic analysis of changes in power did not confirm this pattern (**Fig. S7**). Finally, because gamma-band power is modulated by the phase of low-frequency oscillations (Lakatos et al., 2008), changes in cross-frequency interactions between delta and gamma (e.g. stronger phase-locking of gamma activity) might potentially drive the observed hyper-correlations. Therefore, a precise mechanism behind hyper-correlated gamma-band activity remains to be established.

Importantly, we found changes in power and *coupling strength* also in other frequency bands (see supplementary results for more details). But, first, only delta-band power and gamma-band coupling constitute correlates of conscious states consistent across data sets (**Fig. S7**, **Fig. S8**) and, second, in the anesthesia data-set only high frequency bands exhibited anesthetic-specific effects (**Fig. S9**). Because gamma-band activity is reliably correlated with neuronal firing (Whittingstall and Logothetis, 2009; Le Van Quyen et al., 2016) we hypothesize that gamma amplitude constitutes the best proxy for local activations of brain regions and that might account for robustness of gamma-band results.

Another important feature of gamma-band oscillations is that their amplitude is correlated with amplitude of fMRI BOLD signal (Logothetis et al., 2001; Niessing et al., 2005). He et al. (2008) and Keller et al. (2013) revealed a striking correspondence between patterns of BOLD (anti-)correlations and, specifically, gamma-band amplitude (anti-)correlations. Therefore, an increase in gamma-band coupling might be an electrophysiological process underlying increases in strength of positive correlations (and decreases in strength of negative correlations) of fMRI BOLD signals observed during LOC in several previous studies. Firstly, in rats, isoflurane anesthesia resulted in a spatially non-specific, global increase in strength of positive correlations (Williams et al., 2010). Secondly, in humans, during moderate propofol sedation two regions hypothesized crucial for consciousness - precuneus (Liu et al., 2014) and posterior cingulate cortex (Stamatakis et al. 2010) – exhibited local increase in strength of positive correlations. Thirdly, DMN anti-correlations decreased during propofol anesthesia (Boveroux et al., 2010), ketamine sedation (Bonhomme et al., 2016), N-REM sleep (Samann et al., 2011), and in unresponsive wakefulness syndrome patients (Boly et al., 2009; Di Perri et al., 2016). A relation between changes in gamma-band amplitude-coupling and BOLD correlations is in agreement with Engel et al. (2013), who proposed that whereas the neurophysiological phase-coupling is a distinct mechanism (related to information routing and transfer), both neurophysiological amplitude-correlations and BOLD signal correlations reflect the same modulatory mechanism regulating activation of neuronal populations.

There is considerable literature on neuronal and subjective effects of propofol and ketamine, but

medetomidine has received little attention. Consequently, it is more difficult to interpret the medetomidine-induced effects we observed. In a study of Williams et al. (2010) conducted on rats, sevoflurane anesthesia was accompanied by a pronounced increase in BOLD signal correlations (similar to the propofol-induced effect observed here), but medetomidine resulted in only moderate correlation increase, again in line with the generally moderate effect of medetomidine on gamma-band correlations. However, we found that medetomidine caused an increase in correlations preferentially in frontal and parietal regions, and thus this might be sufficient to cause LOC. Interestingly, the spatial pattern of changes in correlations caused by ketamine+medetomidine seems to result from an additive (linear) effect, rather than an interaction of both anesthetics (**Fig. 5**).

Overall, using two independent datasets, recorded from two different species and involving two different manipulations of consciousness, we revealed hyper-correlated gamma-band activity as a correlate of LOC. Future studies will relate the proposed measure to subjective reports and test its validity in clinical contexts.

# Methods

### Anesthesia data set

The anesthesia dataset analyzed in the present study was recorded at the RIKEN Institute (Japan) and it is publicly available from the Neurotycho database (http://neurotycho.org/). The protocol was approved by the RIKEN Ethics Committee. The following descriptions apply to the original study (Nagasaka et al., 2011; Yanagawa et al., 2013), which should be consulted if additional details are sought. The details of the experiment can be also found online (http://wiki.neurotycho.org/Anesthesia_and_Sleep_Task_Details).

One *macaca mulatta* (S) and three *macaca fuscata* monkeys (G, K, C) took part in the anesthesia study. The study consisted of 22 experimental sessions, each session conducted on a separate day (see: **Table 1**). Four different anesthetic agents were used across sessions: ketamine and medetomidine (KTMD), ketamine (KT), medetomidine (MD), or propofol (PF). Monkeys S and K took part in three experimental sessions each, with KTMD only. Monkeys G and C took part in 8 experimental sessions each, 2 sessions per one anesthetic mix. Anesthetics were injected, either intramuscularly (KTMD, KT, MD) or intravenously (PF).

Electrocorticography (ECoG) data were recorded with a sampling frequency of 1000Hz using a chronically implanted multichannel electrode arrays (Unique Medical, Japan). The arrays, consisting of 128 platinum electrodes spaced with 5mm inter-electrode distance, were implanted in the subdural space and covered the majority of the lateral part of the left hemisphere (**Fig. S1**). In

two monkeys (K and S) the medial cortical regions were also partially covered. Reference electrodes were made of rectangular platinum plates located in the subdural space between the ECoG array and dura. Ground electrodes were placed in the epidural space.

During experiments monkeys were sitting with their head and arms restrained. There was no specific task, thus the recordings can be considered to reflect spontaneous (resting-state) brain activity. In each experimental session ECoG data were recorded during five predefined conditions (states) in the following order:

1. First, a wakefulness (baseline) eyes-open recording lasting between 10-20 minutes was conducted.
2. Next, monkeys were blindfolded and wakefulness (baseline) eyes-closed data were acquired. This period was referred to as *PRE* and used in our analysis as a baseline. Eyes-closed recordings were selected as a baseline as they provide better control when comparing to anesthesia than eyes-open data.
3. Next an anesthetic agent was injected. Beginning of the anesthesia period (*ANES*) was defined as the point at which the monkey did not respond to manipulation of a hand or touching nostrils with a cotton swab. Once unresponsiveness of a monkey was established ECoG data were recorded for around 20-30 minutes in KTMD sessions and around 10-15 minutes in KT, MD, or PF sessions.
4. The recovery from anesthesia was either spontaneous (in KT and PF sessions) or caused by injection of atipamezole, which is an MD antagonist (in KTMD and MD). It was defined as the point at which the monkey started responding to manipulation of the hand or touching of the nostril or philtrum with a cotton swab at same sensitivity as during *PRE* conditions. After establishing the return of responsiveness wakefulness eyes-closed condition was again recorded. This period was used in our analysis and is referred to as *POST*. Of note, one experimental session was missing data recorded after return of responsiveness (see: **Table 1**).
5. As the last step the blindfold was removed from the monkey's eyes and wakefulness eyes-open data were again acquired.

All further analyses were conducted as a part of the present study. Initially the ECoG signals were filtered with a high-pass (0.5Hz, filter order 6600) finite impulse response (FIR) filter, low-pass (125Hz, order 106) FIR filter, and band-stop (48-52Hz, order 1650) FIR filter. The low-pass filtering aimed to prevent aliasing artefacts during subsequent downsampling to 500Hz. These initial preprocessing steps were followed by visual inspection of the data to check for major artefacts. We discarded first 60s of recordings from each condition in order to avoid possible non-

stationarities related to change in the monkey's state. To allow easier inter-subjects comparisons we aimed to obtain signals of the same length and thus, for each subject and condition only the subsequent 420s (7 minutes) of the signal were taken for the further analysis. Preprocessing was conducted with custom-written scripts using eeglab12 functions (Delorme and Makeig, 2004).

**Sleep data set**

Recordings in human epilepsy patients have been conducted as a part of another study (Pigorini et al., 2015). Results from the same data have been already published in Schartner et al. (2017). In agreement with the HORIZON 2020 requirement, the protocol used to collect the patients' data was drawn up in accordance with the EU standards of good clinical practice and with the Declaration of Helsinki (current revision) and is approved by the Ethics Committee of the Niguarda Hospital of Milan (protocol number: ID 939, Niguarda Hospital, Milan, Italy). The data are treated confidentially in compliance with good clinical practice as well as in compliance with Italian specific national laws on the protection of individuals. Patients are informed that personal data are collected and stored electronically, that can be used for purposes of scientific research and that dissemination of the results can take place only in an anonymous and / or aggregate form. Patients are also informed that they have the right to know the data stored, and to update or modify erroneous data.

The data were derived from a dataset collected during the pre-surgical evaluation of ten neurosurgical patients with a history of drug-resistant, focal epilepsy. All subjects were candidates for surgical removal of the epileptogenic zone. The recordings were obtained from stereotactically implanted multi-lead intracerebral electrodes (Stereo-EEG, SEEG), inserted for the precise localization of the epileptogenic zone and connected areas (Arnulfo et al., 2015). The investigated hemisphere, the duration of implantation, the location and number of recording sites were determined based on non-invasive clinical assessment.

SEEG activity was recorded from platinum-iridium semiflexible multi-contact intracerebral electrodes, with a diameter of 0.8mm, a contact length of 1.5mm, an inter-contact distance of 2mm and a maximum of 18 contacts per electrode (Dixi Medical, Besancon France). In addition, scalp EEG activity was recorded from two platinum needle electrodes placed during surgery on the scalp at standard 10-20 positions Fz and Cz. Electro-ocular activity was recorded from the outer canthi of both eyes, and submental electromyographic activity was also recorded. Both EEG and SEEG signals were recorded using a 192-channel recording system (NIHON-KOHDEN NEUROFAX-110) with a sampling rate of 1000 Hz. Data were recorded and exported in EEG Nihon-Kohden format. Recordings were referenced to a contact located entirely in the white matter.

In each subject, recordings were made from up to 194 contacts. Preprocessing and artefacts rejection were performed manually by an expert epileptiologist. Specifically, we excluded from the analysis those contacts that (i) were located in white matter (as assessed by MRI); (ii) were located in the epileptogenic zone (as confirmed by post-surgical assessment); (iii) were located over regions of documented alterations of the cortical tissue (e.g. Focal Cortical Dysplasia; as measured by the radiographic assessment); or (iv) exhibited spontaneous or evoked epileptiform activity during wakefulness or NREM (Valentin et al., 2002). The remaining channels were artefact-free and there was no need to reject any fragments of the signal. The data were imported from EEG Nihon Kohden format into Matlab and converted using a customized Matlab script.

Fragments of sEEG signals were taken from four different states: i) WAKE: resting-state wakefulness, which was recorded at various times of day (between 8 am and 6 pm) with subjects sitting on a bed with eyes closed; ii) REM: a stable episode of rapid-eyes movement sleep; iii) NREM1: the first stable non-rapid eye-movement (stage 3 as defined by Silber et al., 2007) sleep episode at night; iv) NREM2: the last stable stage 3 episode at night. Sleep scoring was obtained according to Silber et al. (2007) using one scalp EEG derivation, together with one bipolar electrooculographic (EOG) and one electromyographic (EMG) derivation. Using only stage 3 we avoided potential fluctuations of consciousness during stage 1 and stage 2 sleep. After preprocessing the length of the retained data sample for each subject and state varied between 7-16min.

Preprocessing of the sleep data set has been done as a part of the Schartner et al. (2017) study. Specifically, bipolar montages were calculated for sEEG data by subtracting the signals from adjacent contacts of the same multi-lead electrode to minimize common electrical noise and to maximize spatial resolution (Cash et al., 2009; Gaillard et al., 2009). To further minimize volume conduction artefacts, at most every third (bipolar) channel from each electrode was retained for analysis. After preprocessing channel selection the following number of bipolarly-referenced channels was retained for 10 included subjects: 22, 23, 18, 22, 23, 28, 31, 29, 25, 26. The data were downsampled to 250Hz. Location of the electrodes is shown in **Fig. 7**. Further details can be also found in Fig. 2 in Schartner et al. (2017), which presents distribution of electrodes according to brain anatomical lobes.

**Functional co-activations (amplitude coupling)**

The analysis pipeline applied to both datasets is schematically depicted in **Fig. 1A**. First, band-pass filtering was used to isolate activity in the low gamma-band (30-45Hz). Next the Hilbert transform was used (Matlab function *hilbert*) to convert band-passed signals to discrete-time

analytic signals for each band. The analytic signals were further down-sampled to 50Hz. We then calculated an absolute value of the complex signals in order to obtain envelopes, which indicate time-resolved instantaneous power of each band. Of note, we restricted our analysis to the low gamma-band, as the Hilbert transform is appropriate for a rather narrow-band signal (when using a wide frequency range the impact of low frequencies is disproportionally strong). Low gamma-band is often associated with 40Hz oscillations (Singer and Gray, 1995; Fries, 2009; Crick and Koch, 1990), and therefore we set the lower cut-off to 30Hz. The upper cut-off was set to 45Hz in order to avoid any influence of the 50Hz line noise.

Further, we aimed to study co-activation between brain regions, here defined as temporal covariation of amplitudes of brain electrical activity (amplitude-coupling). We thus calculated Pearson correlation coefficient (Matlab function *corrcoef*) between the envelopes of every pair of electrodes. In order to capture the supposedly dynamic and transient interactions the covariation was estimated within relatively short (5s long) non-overlapping windows. Thus, the 420s long recordings were divided into 84 windows (in the macaque data set, where data segments of the same length were extracted). Since the sampling frequency of the envelopes was 50Hz, 250 data-points fell within each window. For each pair of channels and each temporal window before estimating the correlation coefficient we first excluded the outliers, which were defined as the data-points > or < than 1.5 standard deviation (*std*) from the mean of a given channel. This way we tried to ascertain that the correlation reflects continuous covariation of the envelopes over the 5s-long interval, rather than brief variations in the amplitude (which could reflect some residual artefacts). We also conducted control analyses with a less conservative criterion (2.5 *std*) or without removing the outlier time-points at all, but this did not significantly affect the main results (data not reported). Calculating correlation coefficient for every pair of electrodes within each window resulted in a 3D matrix (128 X 128 X 84; in the macaque dataset, where 128 channels were always analyzed) of correlation coefficient values ($r$) and a similar matrix of significance values ($p$). Based on the full matrices of $r$-values histograms were created, indicating probability of observing a particular $r$ value across all time-points and electrodes' pairs (**Fig. S2**). Functional co-activations estimated by a correlation coefficient were then represented as sparse, weighted, signed, time-varying networks, where only significant interactions were represented, i.e. when $p<0.05$ the connection maintained its original strength ($r$ value), but when $p>=0.05$ the $r$ value was set to 0 and the connection was considered non-existent. Crucially for our analysis, the networks were signed, i.e. they consisted of both positive ($r>0$) and negative ($r<0$) connections, representing correlations and anti-correlations, respectively.

The primary measure used in our study was *coupling strength,* defined as an average over a full correlation matrix (i.e. both significant and insignificant $r$ values), which might be considered a

single measure of a coupling balance among all brain areas. As our secondary measures we calculated network's *density*, defined as a proportion of existing connections out of all possible connections in the sparse network. Density was calculated separately for positive ($density_+$) and negative ($density_-$) connections. To capture the balance between positive and negative interactions we calculated a proportion of negative to positive connections ($density_- / density_+$).

We report results of two control analyses. First, we investigated how varying the length of a sliding-window used for estimation of correlation coefficients affects the between-conditions differences (**Fig. S6A**). Second, it is known that anesthesia results in substantial changes in the spectral content of brain oscillations. These changes likely affect the observed correlation values. Therefore for each pair of electrodes we created surrogate data by reshuffling the temporal windows and, additionally, we imposed a condition that the windows had to be at least 50s apart. We created 84 pairs of such temporally reshuffled windows to match the number of windows pairs in the original data. Such surrogates allowed estimating the effect of the spectral content on correlation values, as the spectral content was the same in surrogate and original data. Histograms created based on the surrogate data are depicted in **Fig. S2**. We created surrogate-corrected results by subtracting, for each sessions and condition, *coupling strength* estimated from surrogates from original *coupling strength*, and thus correcting for potential biases resulting from different spectral properties (**Fig. S6B**).

**Anatomical modules**

In order to investigate the effects of anesthesia on different cortical regions we assigned the electrodes used for ECoG recordings into five modules identified in the macaque anatomical brain network. The anatomical modules were investigated in an already published study of Goulas et al (2014), who estimated the modular structure of the anatomical network based on the dataset and atlas described in Markov et al (2014). The Markov et al (2014) dataset was derived from gold-standard tract-tracing techniques and offers the complete picture of the anatomical connections between 29 cortical areas. Hence, based on the Markov et al (2014) data Goulas et al (2014) constructed a 29x29 directed and weighted graph representing underlying anatomical network and used a spectral decomposition algorithm in order to detect the network's modular structure. The resulting modules were mapped to the atlas of Markov et al 2014 in F99 space. We used the spatial locations of the ECoG electrodes and macroscopic landmarks of the macaque cortex to assign ECoG electrodes to the anatomically defined modules found by Goulas et al. (2014). Electrodes with ambiguous location were left unassigned (see **Fig S1**). This allowed comparing the effects of anesthetics within different cortical areas. For details of the anatomical dataset see Markov et al

(2014), and for details of the anatomical network modular decomposition see Goulas et al (2014).

**Statistical analysis**

We applied the following statistical analyses to spectral power, *coupling strength*, $density_{+}$, and $density_{-}$. In **Fig. 3**, **6**, **S7**, and **S8** we compared scalar values of measures (calculated as an average over electrodes and then median over time-points) among conditions. First, distribution of each measure was tested within each condition with the Kolmogorov-Smirnoff test. Repeated-measures ANOVA was used when all conditions had a Gaussian distribution, and non-parametric Friedman test was used otherwise. When significant effect of a state was found pairwise post-hoc comparisons were conducted between conditions using either parametric paired-samples t-tests or non-parametric Wilcoxon tests. Post-hoc tests were corrected for a number of comparisons (3 in the anesthesia data-set, 6 in the sleep data-set) using the Bonferroni-Holm procedure (Holm, 1979). A standardized difference score ($d_z$) was calculated as an indicator of the effect size (Cohen, 1988) and defined as $d_z$ = abs(mean(X1 - X2) / std(X1 - X2)) * sqrt(2), where X1 and X2 are values of a measure from two compared conditions.

In **Fig. 4** and **S9** we estimated Cohen's *d* indicating effect size for comparisons between PRE and ANES within each session. Specifically, we took advantage of the fact that all measures were estimated in a time-varying manner (i.e. within 5 s long time-windows) and used within-conditions variability across time-points to estimate Cohen's *d*, which was defined as *d* = abs(mean(X1) - mean(X2)) / sqrt((std(X1) - std(X2)) /2) ), where X1 and X2 are time-resolved estimates of a measure from two compared conditions.

In **Fig. 5** we investigated topographic effects of anesthesia and analyzed time-resolved nodal *coupling strength* (*nCS*) for each electrode (i.e. we obtained a 128X84 *nCS* matrix). Next for each experimental session we calculated a $\Delta nCS_{Diff}$ matrix by subtracting median($nCS_{PRE}$) from $nCS_{ANES}$. A vector $\Delta nCS_{AvDiff}$, indicating an average change over PRE baseline was then calculated by averaging $\Delta nCS_{Diff}$ over time. Topographic plots of $\Delta nCS_{AvDiff}$ for moneys C and G can be found in **Fig. 5A**. In order to emphasize the topographic distribution of changes the color-coding was adjusted within each session between: [max($\Delta nCS_{AvDiff}$)*-1, max($\Delta nCS_{AvDiff}$)]. In **Fig. 5B** (upper panel) we plotted $\Delta nCS_{AvDiff}$ averaged over electrodes assigned to frontal, parieto-motor, and occipital anatomical modules. The *p* values presented in **Fig. 5B** were calculated by averaging $\Delta nCS_{Diff}$ over electrodes from a given anatomical module and comparing the time-resolved (but averaged over electrodes) values against zero using a one-sample Wilcoxon test. In **Fig. S4** we present results of statistical analysis conducted in the same way, but for single electrodes (rather than for data averaged within anatomical modules).

**Fig. 5C** shows results of a hierarchical agglomerative clustering procedure assessing similarity of anesthesia-related changes in spatial patterns of gamma-band correlations. The $\Delta nCS_{AvDiff}$ vectors were z-score normalized in order to emphasize spatial, rather than absolute differences and the Euclidean distance between pairs of normalized vectors was estimated. Next the vectors were clustered based on the Ward's criterion (Matlab function *linkage*). The distance between vectors and the results of clustering were plotted in the form of dendrograms (Matlab function *dendrogram*). This analysis was possible only within subjects due to differences in spatial arrangements of the ECoG electrodes between subjects.

# References


Akeju, O., Song, A. H., Hamilos, A. E., Pavone, K. J., Flores, F. J., Brown, E. N., & Purdon, P. L. (2016). Electroencephalogram signatures of ketamine anesthesia-induced unconsciousness. *Clinical Neurophysiology*, *127*(6), 2414-2422.

Alonso, L. M., Proekt, A., Schwartz, T. H., Pryor, K. O., Cecchi, G. A., & Magnasco, M. O. (2014). Dynamical criticality during induction of anesthesia in human ECoG recordings. *Frontiers in Neural Circuits*, *8*.

Arnulfo, G., Hirvonen, J., Nobili, L., Palva, S., & Palva, J. M. (2015). Phase and amplitude correlations in resting-state activity in human stereotactical EEG recordings. *Neuroimage*, *112*, 114-127.

Baars, B. J. (2005). Global workspace theory of consciousness: toward a cognitive neuroscience of human experience. *Progress in Brain Research*, *150*, 45-53.

Bekinschtein, T. A., Shalom, D. E., Forcato, C., Herrera, M., Coleman, M. R., Manes, F. F., & Sigman, M. (2009). Classical conditioning in the vegetative and minimally conscious state. *Nature Neuroscience*, *12*(10), 1343-1349.

Blain-Moraes, S., Lee, U., Ku, S., Noh, G., & Mashour, G. A. (2014). Electroencephalographic effects of ketamine on power, cross-frequency coupling, and connectivity in the alpha bandwidth. *Frontiers in Systems Neuroscience*, *8*, 114.

Boly, M., et al. (2009). Functional connectivity in the default network during resting state is preserved in a vegetative but not in a brain dead patient. *Human Brain Mapping*, *30*(8), 2393-2400.

Boly, M., Garrido, M. I., Gosseries, O., Bruno, M. A., Boveroux, P., Schnakers, C., ... & Friston, K. (2011). Preserved feedforward but impaired top-down processes in the vegetative state. *Science*, *332*(6031), 858-862.

650 Boly, M., Moran, R., Murphy, M., Boveroux, P., Bruno, M. A., Noirhomme, Q., ... & Laureys, S.
651 (2012). Connectivity changes underlying spectral EEG changes during propofol-induced loss of
652 consciousness. *Journal of Neuroscience*, *32*(20), 7082-7090.
653 Bonhomme, V., et al. (2016). Resting-state network-specific breakdown of functional connectivity
654 during ketamine alteration of consciousness in volunteers. *The Journal of the American Society of*
655 *Anesthesiologists*, *125*(5), 873-888.
656 Boveroux, P., et al. (2010). Breakdown of within-and between-network resting state functional
657 magnetic resonance imaging connectivity during propofol-induced loss of consciousness. *The Journal*
658 *of the American Society of Anesthesiologists*, *113*(5), 1038-1053.
659 Brown, E. N., Lydic, R., & Schiff, N. D. (2010). General anesthesia, sleep, and coma. *New*
660 *England Journal of Medicine*, *363*(27), 2638-2650.
661 Casali, A. G., et al. (2013). A theoretically based index of consciousness independent of sensory
662 processing and behavior. *Science Translational Medicine*, *5*(198), 198ra105-198ra105.
663 Cash, S.S., et al. 2009. The human K-complex represents an isolated cortical down-state. *Science*
664 324, 1084-1087. http://dx.doi.org/10.1126/science.1169626.
665 Chennu, S., O'Connor, S., Adapa, R., Menon, D. K., & Bekinschtein, T. A. (2016). Brain
666 Connectivity Dissociates Responsiveness from Drug Exposure during Propofol-Induced Transitions
667 of Consciousness. *PLoS Comput Biol*, *12*(1), e1004669.
668 Chialvo, D. R. (2010). Emergent complex neural dynamics. *Nature Physics*, *6*(10), 744-750.
669 Coleman, M. R., Rodd, J. M., Davis, M. H., Johnsrude, I. S., Menon, D. K., Pickard, J. D., &
670 Owen, A. M. (2007). Do vegetative patients retain aspects of language comprehension? Evidence
671 from fMRI. *Brain*, *130*(10), 2494-2507.
672 Collier, B. B. (1972). Ketamine and the conscious mind. *Anesthesia*, *27*(2), 120-134.
673 Cruse, D., et al. (2012). Bedside detection of awareness in the vegetative state: a cohort study. *The*
674 *Lancet*, *378*(9809), 2088-2094.
675 Dehaene, S. & Changeux, J. P. (2011). Experimental and theoretical approaches to conscious
676 processing. *Neuron*, *70*(2), 200-227.
677 Delorme, A., & Makeig, S. (2004). EEGLAB: an open source toolbox for analysis of single-trial
678 EEG dynamics including independent component analysis. *Journal of Neuroscience Methods*, *134*(1),
679 9-21.
680 Di Perri, C., et al. (2016). Neural correlates of consciousness in patients who have emerged from a
681 minimally conscious state: a cross-sectional multimodal imaging study. *The Lancet Neurology*, *15*(8),
682 830-842.
683 Engel, A. K., Gerloff, C., Hilgetag, C. C., & Nolte, G. (2013). Intrinsic coupling modes: multiscale

684 interactions in ongoing brain activity. *Neuron*, *80*(4), 867-886
685 Fernández-Espejo, D., & Owen, A. M. (2013). Detecting awareness after severe brain
686 injury. *Nature Reviews Neuroscience*, *14*(11), 801-809.
687 Franks, N. P. (2008). General anesthesia: from molecular targets to neuronal pathways of sleep and
688 arousal. *Nature Reviews Neuroscience*, *9*(5), 370-386.
689 Fries, P. (2009). Neuronal gamma-band synchronization as a fundamental process in cortical
690 computation. *Annual Review of Neuroscience*, *32*, 209-224.
691 Gaillard, R., Dehaene, S., Adam, C., Clemenceau, S., Hasboun, D., Baulac, M., Cohen, L.,
692 Naccache, L., 2009. Converging intracranial markers of conscious access. PLoS Biol. 7, e61.
693 Garfield, J. M., Garfield, F. B., Stone, J. G., Hopkins, D., & Johns, L. A. (1972). A comparison of
694 psychologic responses to ketamine and thiopental–nitrous oxide–halothane anesthesia. *The Journal of*
695 *the American Society of Anesthesiologists*, *36*(4), 329-338.
696 Goulas, A., Schaefer, A., & Margulies, D. S. (2015). The strength of weak connections in the
697 macaque cortico-cortical network. *Brain Structure and Function*, *220*(5), 2939-2951.
698 Hanley, J. A., & McNeil, B. J. (1982). The meaning and use of the area under a receiver operating
699 characteristic (ROC) curve. *Radiology*, *143*(1), 29-36.
700 He, B. J., Snyder, A. Z., Zempel, J. M., Smyth, M. D., & Raichle, M. E. (2008).
701 Electrophysiological correlates of the brain's intrinsic large-scale functional architecture. *Proceedings*
702 *of the National Academy of Sciences USA*, *105*(41), 16039-16044.
703 Keller, C. J., et al. (2013). Neurophysiological investigation of spontaneous correlated and
704 anticorrelated fluctuations of the BOLD signal. *The Journal of Neuroscience*, *33*(15), 6333-6342.
705 King, J. R., Sitt, J. D., Faugeras, F., Rohaut, B., El Karoui, I., Cohen, L., ... & Dehaene, S. (2013).
706 Information sharing in the brain indexes consciousness in noncommunicative patients. *Current*
707 *Biology*, *23*(19), 1914-1919.
708 Koch, C., Massimini, M., Boly, M., & Tononi, G. (2016). Neural correlates of consciousness:
709 progress and problems. *Nature Reviews Neuroscience*, *17*(5), 307-321.
710 Kouider, S., & Dehaene, S. (2007). Levels of processing during non-conscious perception: a
711 critical review of visual masking. *Philosophical Transactions of the Royal Society B: Biological*
712 *Sciences*, *362*(1481), 857-875.
713 Krzemiński, D., Kamiński, M., Marchewka, A., & Bola, M. (2017). Breakdown of long-range
714 temporal correlations in brain oscillations during general anesthesia. *Neuroimage*.
715 Krystal, J. H., et al. (1994). Subanesthetic effects of the noncompetitive NMDA antagonist,
716 ketamine, in humans: psychotomimetic, perceptual, cognitive, and neuroendocrine
717 responses. *Archives of General Psychiatry*, *51*(3), 199-214.

718 Ku, S. W., Lee, U., Noh, G. J., Jun, I. G., & Mashour, G. A. (2011). Preferential inhibition of
719 frontal-to-parietal feedback connectivity is a neurophysiologic correlate of general anesthesia in
720 surgical patients. *PloS one*, *6*(10), e25155.
721 Lakatos, P., Karmos, G., Mehta, A. D., Ulbert, I., & Schroeder, C. E. (2008). Entrainment of
722 neuronal oscillations as a mechanism of attentional selection. *Science*, *320*(5872), 110-113.
723 Le Van Quyen, M., et al. (2016). High-frequency oscillations in human and monkey neocortex
724 during the wake–sleep cycle. *Proceedings of the National Academy of Sciences USA*, *113*(33), 9363-
725 9368.
726 Lee, U., Ku, S., Noh, G., Baek, S., Choi, B., & Mashour, G. A. (2013). Disruption of frontal–
727 parietal communication by ketamine, propofol, and sevoflurane. *The Journal of the American Society*
728 *of Anesthesiologists*, *118*(6), 1264-1275.
729 Lewis, L. D., et al. (2012). Rapid fragmentation of neuronal networks at the onset of propofol-
730 induced unconsciousness. *Proceedings of the National Academy of Sciences USA*, *109*(49), E3377-
731 E3386.
732 Liu, X., Li, S. J., & Hudetz, A. G. (2014). Increased precuneus connectivity during propofol
733 sedation. *Neuroscience Letters*, *561*, 18-23.
734 Logothetis, N. K., Pauls, J., Augath, M., Trinath, T., & Oeltermann, A. (2001). Neurophysiological
735 investigation of the basis of the fMRI signal. *Nature*, *412*(6843), 150-157.
736 Lydic, R., & Baghdoyan, H. A. (2005). Sleep, anesthesiology, and the neurobiology of arousal
737 state control. *The Journal of the American Society of Anesthesiologists*, *103*(6), 1268-1295.
738 MacDonald, A. A., Naci, L., MacDonald, P. A., & Owen, A. M. (2015). Anesthesia and
739 neuroimaging: investigating the neural correlates of unconsciousness. *Trends in Cognitive*
740 *Sciences*, *19*(2), 100-107.
741 Markov, N. T., et al. (2012). A weighted and directed interareal connectivity matrix for macaque
742 cerebral cortex. *Cerebral Cortex*, bhs270.
743 Massimini, M., Ferrarelli, F., Huber, R., Esser, S. K., Singh, H., & Tononi, G. (2005). Breakdown
744 of cortical effective connectivity during sleep. *Science*, *309*(5744), 2228-2232.
745 Massimini, M., Ferrarelli, F., Murphy, M. J., Huber, R., Riedner, B. A., Casarotto, S., & Tononi,
746 G. (2010). Cortical reactivity and effective connectivity during REM sleep in humans. *Cognitive*
747 *Neuroscience*, *1*(3), 176-183.
748 Monti, M. M., et al. (2010). Willful modulation of brain activity in disorders of
749 consciousness. *New England Journal of Medicine*, *362*(7), 579-589.
750 Naci, L., Cusack, R., Anello, M., & Owen, A. M. (2014). A common neural code for similar
751 conscious experiences in different individuals. *Proceedings of the National Academy of*

752 *Sciences*, *111*(39), 14277-14282.
753 Nagasaka, Y., Shimoda, K., & Fujii, N. (2011). Multidimensional recording (MDR) and data
754 sharing: an ecological open research and educational platform for neuroscience. *PloS One*, *6*(7),
755 e22561.
756 Nieminen, J. O., et al. (2016). Consciousness and cortical responsiveness: a within-state study
757 during non-rapid eye movement sleep. *Scientific Reports*, *6*.
758 Niessing, J., Ebisch, B., Schmidt, K. E., Niessing, M., Singer, W., & Galuske, R. A. (2005).
759 Hemodynamic signals correlate tightly with synchronized gamma oscillations. *Science*, *309*(5736),
760 948-951.
761 Nir, Y., & Tononi, G. (2010). Dreaming and the brain: from phenomenology to
762 neurophysiology. *Trends in Cognitive Sciences*, *14*(2), 88-100.
763 Nir, Y., Staba, R. J., Andrillon, T., Vyazovskiy, V. V., Cirelli, C., Fried, I., & Tononi, G. (2011).
764 Regional slow waves and spindles in human sleep. *Neuron*,*70*(1), 153-169.
765 Owen, A. M., Coleman, M. R., Boly, M., Davis, M. H., Laureys, S., & Pickard, J. D. (2006).
766 Detecting awareness in the vegetative state. *Science*, *313*(5792), 1402-1402.
767 Pigorini, A., et al. (2015). Bistability breaks-off deterministic responses to intracortical stimulation
768 during non-REM sleep. *Neuroimage*, *112*, 105-113.
769 Popa, D., Popescu, A. T., & Paré, D. (2009). Contrasting activity profile of two distributed cortical
770 networks as a function of attentional demands. *The Journal of Neuroscience*, *29*(4), 1191-1201.
771 Purdon, P. L., et al. (2013). Electroencephalogram signatures of loss and recovery of consciousness
772 from propofol. *Proceedings of the National Academy of Sciences USA*, *110*(12), E1142-E1151.
773 Rubinov, M., & Sporns, O. (2011). Weight-conserving characterization of complex functional
774 brain networks. *Neuroimage*, *56*(4), 2068-2079.
775 Sämann, P. G., et al. (2011). Development of the brain's default mode network from wakefulness
776 to slow wave sleep. *Cerebral Cortex*, bhq295.
777 Sanders, R. D., Tononi, G., Laureys, S., & Sleigh, J. W. (2012). Unresponsiveness≠
778 unconsciousness. *The Journal of the American Society of Anesthesiologists*, *116*(4), 946-959.
779 Sarà, M., & Pistoia, F. (2010). Complexity loss in physiological time series of patients in a
780 vegetative state. *Nonlinear dynamics, psychology, and life sciences*, *14*(1), 1.
781 Sarasso, S. et al. (2015). Consciousness and complexity during unresponsiveness induced by
782 propofol, xenon, and ketamine. *Current Biology*, *25*(23), 3099-3105.
783 Schartner, M. M., et al. (2016). Global and local complexity of intracranial EEG decreases during
784 NREM sleep. *Neuroscience of Consciousness*.
785 Schartner, M., Seth, A., Noirhomme, Q., Boly, M., Bruno, M. A., Laureys, S., & Barrett, A.

(2015). Complexity of multi-dimensional spontaneous EEG decreases during propofol induced general anesthesia. *PloS One*, *10*(8), e0133532.

Seth, A. (2009). Explanatory correlates of consciousness: theoretical and computational challenges. *Cognitive Computation*, *1*(1), 50-63.

Seth, A. K., Barrett, A. B., & Barnett, L. (2011). Causal density and integrated information as measures of conscious level. *Philosophical Transactions of the Royal Society of London A: Mathematical, Physical and Engineering Sciences*, *369*(1952), 3748-3767.

Siclari, F., LaRocque, J. J., Postle, B. R., & Tononi, G. (2013). Assessing sleep consciousness within subjects using a serial awakening paradigm. *Frontiers in Psychology*, *4*, 542.

Siclari, F., Baird, B., Perogamvros, L., Bernardi, G., LaRocque, J. J., Riedner, B., ... & Tononi, G. (2017). The neural correlates of dreaming. *Nature Neuroscience*.

Silber, M. H., et al. (2007). The visual scoring of sleep in adults. *J Clin Sleep Med*, *3*(2), 121-131.

Solovey, G., Alonso, L. M., Yanagawa, T., Fujii, N., Magnasco, M. O., Cecchi, G. A., & Proekt, A. (2015). Loss of consciousness is associated with stabilization of cortical activity. *The Journal of Neuroscience*, *35*(30), 10866-10877.

Solt, K., & Forman, S. A. (2007). Correlating the clinical actions and molecular mechanisms of general anesthetics. *Current Opinion in Anesthesiology*, *20*(4), 300-306.

Stamatakis, E. A., Adapa, R. M., Absalom, A. R., & Menon, D. K. (2010). Changes in resting neural connectivity during propofol sedation. *PloS One*, *5*(12), e14224.

Supp, G. G., Siegel, M., Hipp, J. F., & Engel, A. K. (2011). Cortical hypersynchrony predicts breakdown of sensory processing during loss of consciousness. *Current Biology*, *21*(23), 1988-1993.

Tajima, S., Yanagawa, T., Fujii, N., & Toyoizumi, T. (2015). Untangling brain-wide dynamics in consciousness by cross-embedding. *PLoS Comput Biol*, *11*(11), e1004537.

Teasdale, G., & Jennett, B. (1974). Assessment of coma and impaired consciousness: a practical scale. *The Lancet*, *304*(7872), 81-84.

Tononi, G., & Edelman, G. M. (1998). Consciousness and complexity. *Science*, *282*(5395), 1846-1851.

Tononi, G. (2004). An information integration theory of consciousness. *BMC neuroscience*, *5*(1), 42.

Tononi, G., Boly, M., Massimini, M., & Koch, C. (2016). Integrated information theory: from consciousness to its physical substrate. *Nature Reviews Neuroscience*.

Vizuete, J. A., Pillay, S., Ropella, K. M., & Hudetz, A. G. (2014). Graded defragmentation of cortical neuronal firing during recovery of consciousness in rats. *Neuroscience*, *275*, 340-351.

Wang, J., Noh, G. J., Choi, B. M., Ku, S. W., Joo, P., Jung, W. S., Kim, S., & Lee, H. (2017).

Suppressed neural complexity during ketamine-and propofol-induced unconsciousness. *Neuroscience Letters*, *653*, 320-325.

Whittingstall, K. & Logothetis, N. K. (2009). Frequency-band coupling in surface EEG reflects spiking activity in monkey visual cortex. *Neuron*, *64*(2), 281-289.

Williams, K. A., Magnuson, M., Majeed, W., LaConte, S. M., Peltier, S. J., Hu, X., & Keilholz, S. D. (2010). Comparison of α-chloralose, medetomidine and isoflurane anesthesia for functional connectivity mapping in the rat. *Magnetic Resonance Imaging*, *28*(7), 995-1003.

Yanagawa, T., Chao, Z. C., Hasegawa, N., & Fujii, N. (2013). Large-scale information flow in conscious and unconscious states: an ECoG study in monkeys. *PloS One*, *8*(11), e80845.

**Figure 1. A)** Scheme of the data analysis pipeline. (1) Raw EEG signals were (2) band-pass filtered in the low gamma frequency-range (30-45Hz) and Hilbert-transformed in order to obtain an envelope (in red), which indicates the instantaneous amplitude of gamma-band activity. Temporal covariation of envelopes was assessed between all pairs of channels with a Pearson correlation coefficient. To capture the dynamic and transient aspect of brain interactions, correlations between envelopes were estimated within 5s-long sliding windows (t1, t2, t3,…). (3) This resulted in a full correlation matrix for each temporal window (in the scheme different *r* values are represented by colors). C*oupling strength* was then defined as an average over all pairwise correlation coefficient values (i.e. over the full correlation matrices). (4) Next, correlation matrices were represented as sparse co-activation networks, where only significant correlations ($p<0.05$), either positive (red) or negative (blue), between electrodes (represented by black circles) were maintained. *Density,* which indicates the proportion of significant correlations out of all possible correlations, was then calculated, separately for positive and negative connections. **B)** Three postulated categories of consciousness – conscious, unresponsive, and loss of consciousness.

**Figure 2.** Temporal dynamics of gamma-band *coupling strength* within experimental sessions. Two sessions, in which monkey Chibi was anesthetized either with ketamine (KT) or propofol (PF), were chosen as representative examples. The black line indicates *coupling strength* with each data-point reflecting *coupling strength* estimated within a 5 s long sliding window. The horizontal lines below indicate the state of the monkey (PRE – awake baseline; ANES –anesthesia-induced unresponsiveness; POST – awake after return of responsiveness) and the magenta point the moment of anesthetic injection. The histograms on the right side indicate probability of observing a given value of *coupling strength* in each state. The numbered vertical ticks mark time-points (windows) for which topographic maps of nodal *coupling strength* were plotted. Please note the different scale in the topographic maps of KT and PF sessions.

**Figure 3.** Gamma-band power and co-activations during wakefulness and anesthesia – data from macaque monkeys. Four measures are presented: spectral power (**A**), *coupling strength* (**B**), positive correlations ($density_+$; **C**), and proportion of negative (anti-) correlations (i.e. $density_-/density_+$; **D**). In the left panel each triplet of data-points on the *x* axis represents three states (PRE, ANES, POST) from one experimental session. In the right panel the same data are re-plotted - data points joined by a line represent one experimental session and colors distinguish between monkeys. Please note missing *post* data in one of monkey C's experimental sessions.

**Figure 4**. Anesthetics-specific effects on gamma-band power and co-activations. (**A-D**) Changes over pre-anesthesia baseline (i.e. ANES – PRE) are presented. Each marker represents one experimental session, marker's color indicates the monkey, while the shape indicates whether or not the effect size (Cohen's *d*) of within-subject comparison between ANES and PRE was greater than 0.6.

**Figure 5**. Effects of different anesthetics on topography of gamma-band co-activations. **A**)

Anesthesia-related changes in gamma-band *coupling strength* over pre-anesthesia baseline (i.e. ANES – PRE) are presented for two monkeys anesthetized with all four anesthetic agents (C and G). Each map presents results from one experimental session. Greater values, reflected by more intense red color, indicate that a given electrode exhibited greater increase in correlation coefficient values during anesthesia. In order to emphasize spatial, rather than absolute effects, the data were normalized within each session. **B**) Change in nodal (local) *coupling strength* plotted for frontal (Fr.), parieto-motor (Par.), and occipital (Occ.) modules. Here data from monkeys K and S are also included. Each triplet of data-points joined by a line represents one experimental session. Filled circles indicate significant ($p<0.05$; Bonferroni corrected) change over baseline. Assignment of electrodes into specific modules can be found in Fig. S1. **C**) Dendrograms indicating similarity of topographical patterns of changes caused by various anesthetic agents. This analysis was conducted only within subjects due to different localization of the ECoG electrodes across monkeys.

**Figure 6**. Gamma-band power and co-activations during wakefulness and sleep – data from 10 human subjects. The same four measures are plotted in the same convention as in **Fig. 3**.

**Figure 7.** Changes in gamma-band nodal *coupling strength* during sleep. In **A** changes observed during NREM1 in comparison to wakefulness (NREM1 - WAKE) plotted individually for each subject. In **B** differences between conditions plotted collectively for all subjects. R-right; L-left; D-dorsal; V-ventral; P-posterior; A-anterior.

**Figure 8.** Gamma-band co-activations allow reliable discrimination between conditions. Receiver Operating Characteristic (ROC) curves were calculated for comparisons of *coupling strength* between conditions, both at the individual and group level, and area under the curve (AUC) was taken as an indicator of discriminative power.

A

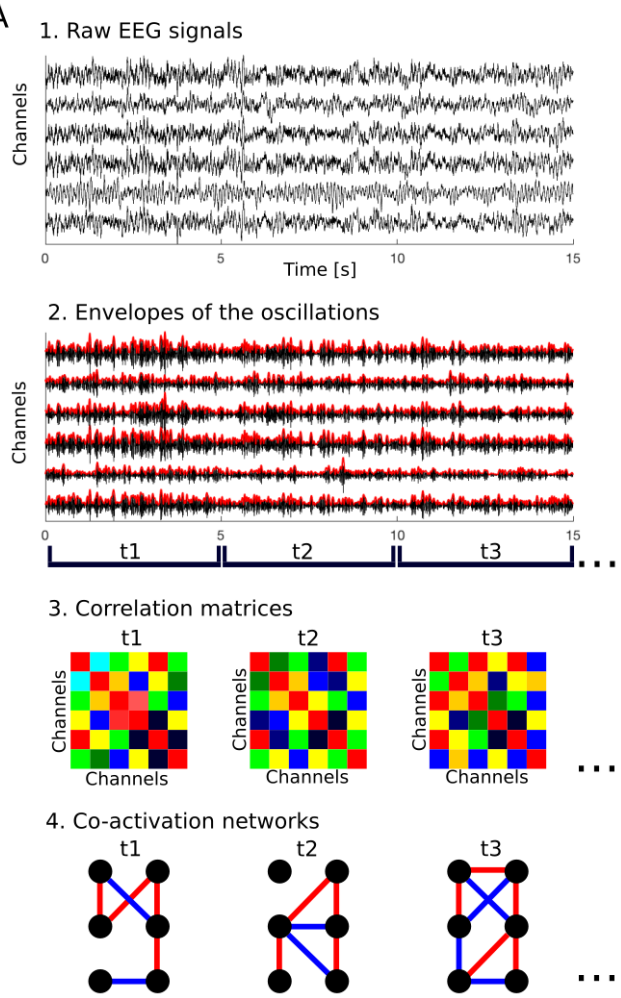


B

| Category | Conscious | Unresponsive | Loss of consciousness |
|---|---|---|---|
| Example | Wakefulness | REM sleep<br>Ketamine anesthesia | N-REM sleep<br>Propofol anesthesia |
| Consciousness | YES | YES | NO |
| Perception | YES | NO | NO |
| Responsiveness | YES | NO | NO |

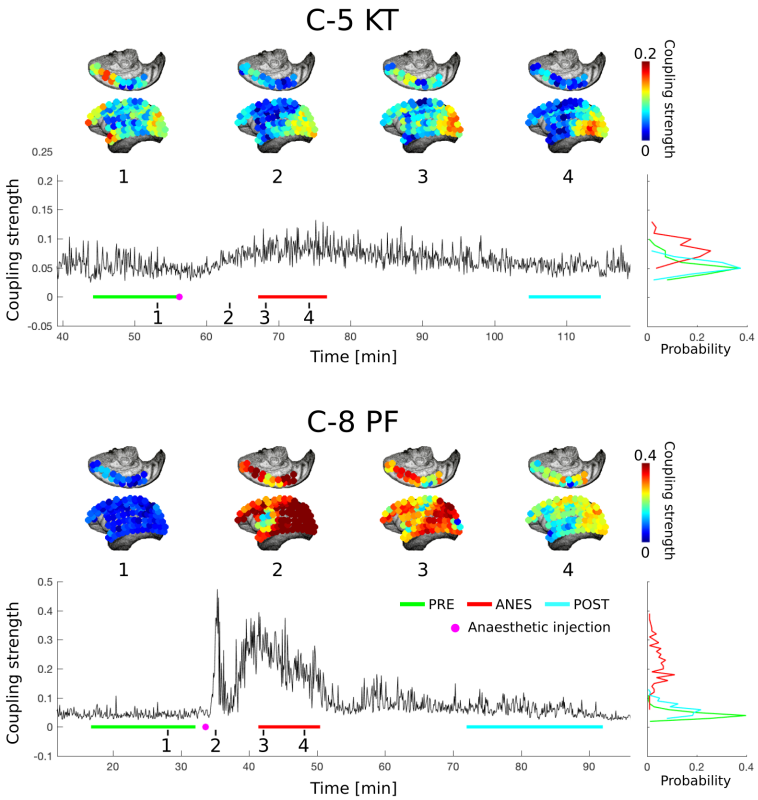
C-5 KT
0.2
Coupling strength
0
1
2
3
4
Coupling strength
Time [min]
Probability
C-8 PF
0.4
Coupling strength
0
PRE
ANES
POST
Anaesthetic injection
Coupling strength
Time [min]
Probability

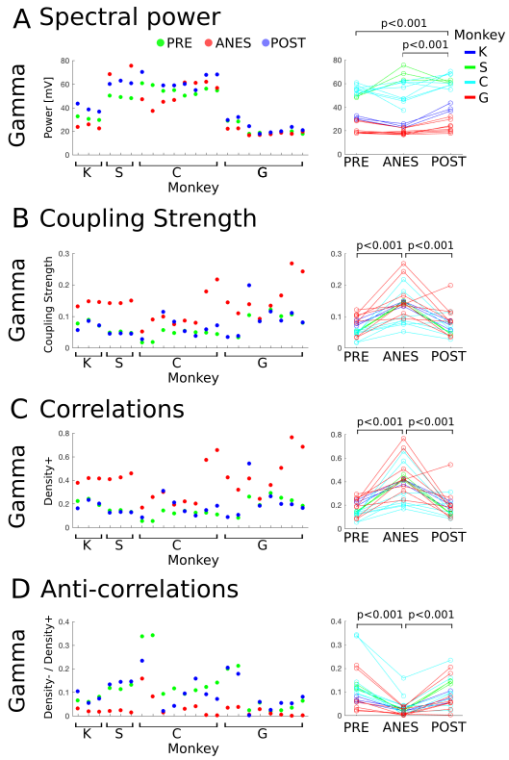
A Spectral power
PRE ANES POST
Gamma
Power [mV]
K S C G
Monkey
p<0.001
p<0.001
Monkey
K
S
C
G
PRE ANES POST
B Coupling Strength
Gamma
Coupling Strength
p<0.001 p<0.001
C Correlations
Gamma
Density+
p<0.001 p<0.001
D Anti-correlations
Gamma
Density- / Density+
p<0.001 p<0.001

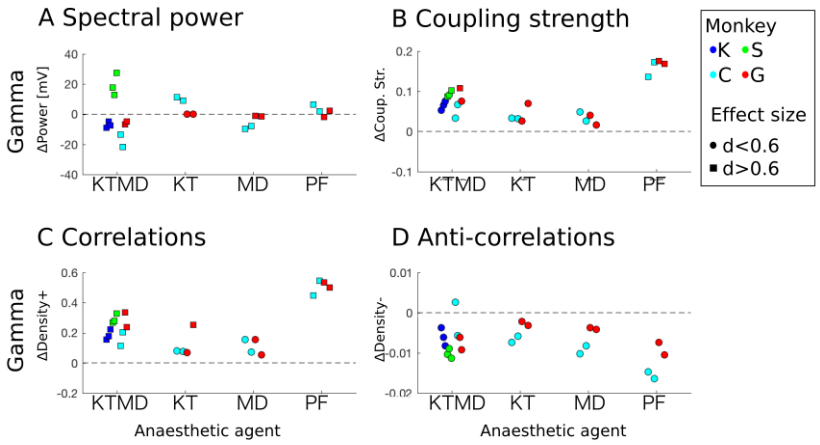
A Spectral power
B Coupling strength
C Correlations
D Anti-correlations
Gamma
ΔPower [mV]
ΔCoup. Str.
ΔDensity+
ΔDensity-
KTMD
KT
MD
PF
Anaesthetic agent
Monkey
K
S
C
G
Effect size
d<0.6
d>0.6

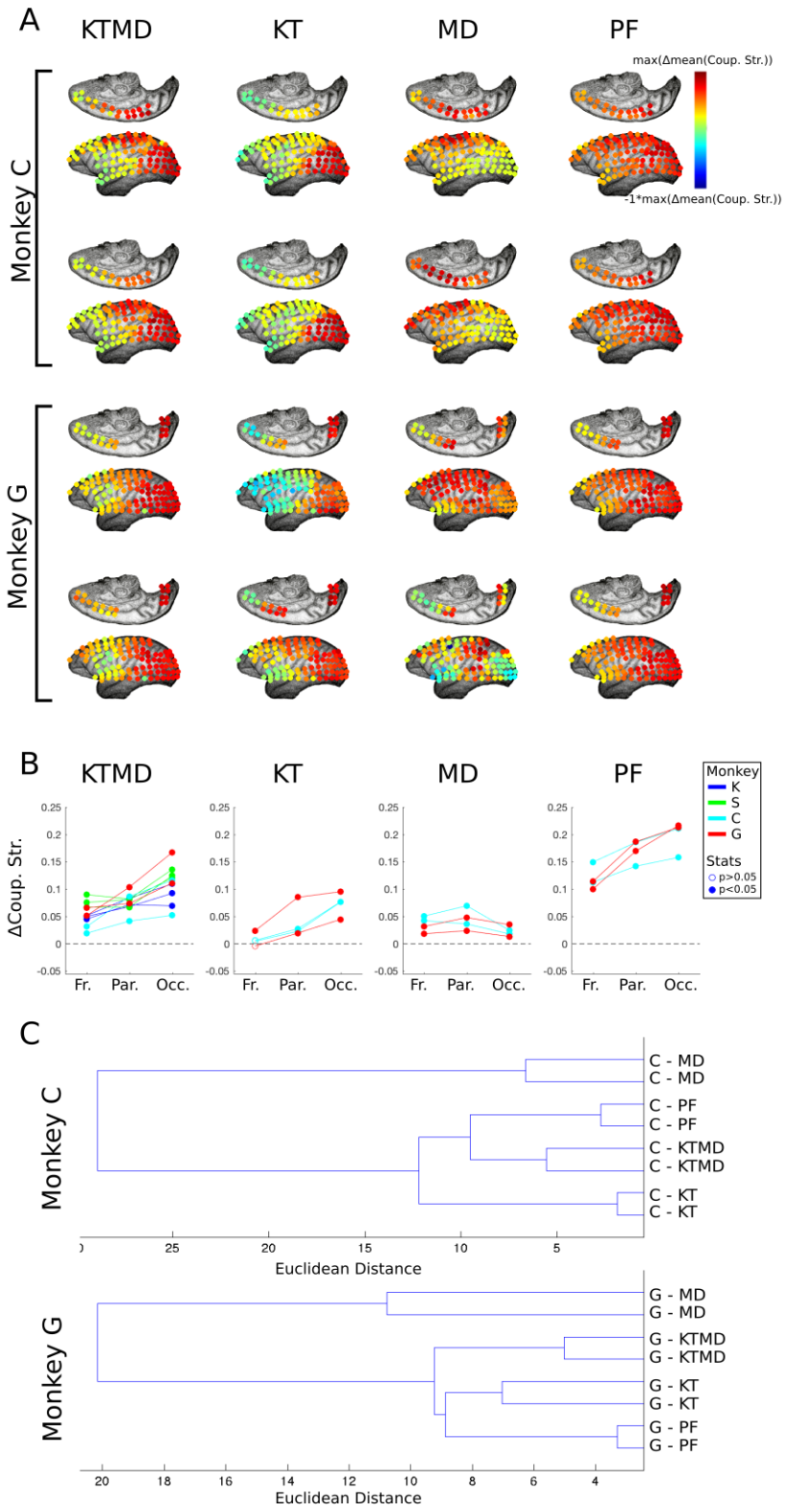
A
KTMD
KT
MD
PF
max(Δmean(Coup. Str.))
-1*max(Δmean(Coup. Str.))
Monkey C
Monkey G
B
KTMD
KT
MD
PF
ΔCoup. Str.
Fr.
Par.
Occ.
Monkey
K
S
C
G
Stats
p>0.05
p<0.05
C
Monkey C
C - MD
C - MD
C - PF
C - PF
C - KTMD
C - KTMD
C - KT
C - KT
Euclidean Distance
Monkey G
G - MD
G - MD
G - KTMD
G - KTMD
G - KT
G - KT
G - PF
G - PF
Euclidean Distance

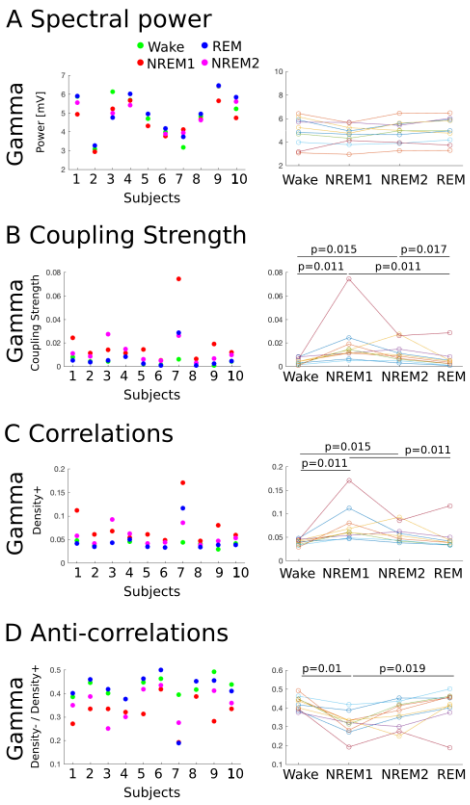
A Spectral power
Wake
REM
NREM1
NREM2
Gamma
Power [mV]
Subjects
Wake NREM1 NREM2 REM
B Coupling Strength
Gamma
Coupling Strength
p=0.015
p=0.017
p=0.011
p=0.011
Subjects
Wake NREM1 NREM2 REM
C Correlations
Gamma
Density+
p=0.015
p=0.011
p=0.011
Subjects
Wake NREM1 NREM2 REM
D Anti-correlations
Gamma
Density- / Density+
p=0.01
p=0.019
Subjects
Wake NREM1 NREM2 REM

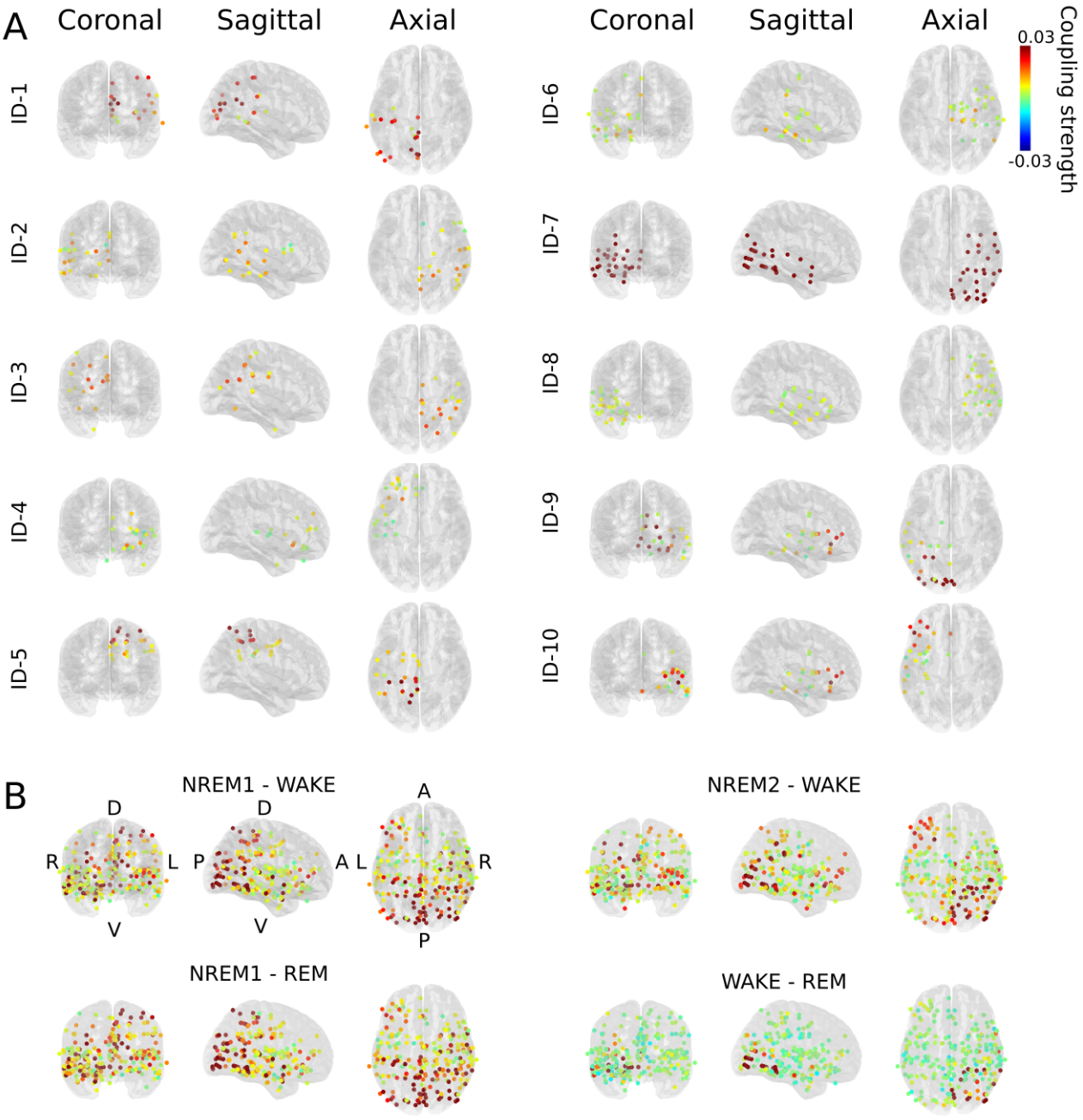
A
Coronal
Sagittal
Axial
ID-1
ID-2
ID-3
ID-4
ID-5
ID-6
ID-7
ID-8
ID-9
ID-10
0.03
-0.03
Coupling strength
B
NREM1 - WAKE
NREM2 - WAKE
NREM1 - REM
WAKE - REM
D
V
R
L
P
A

970
971

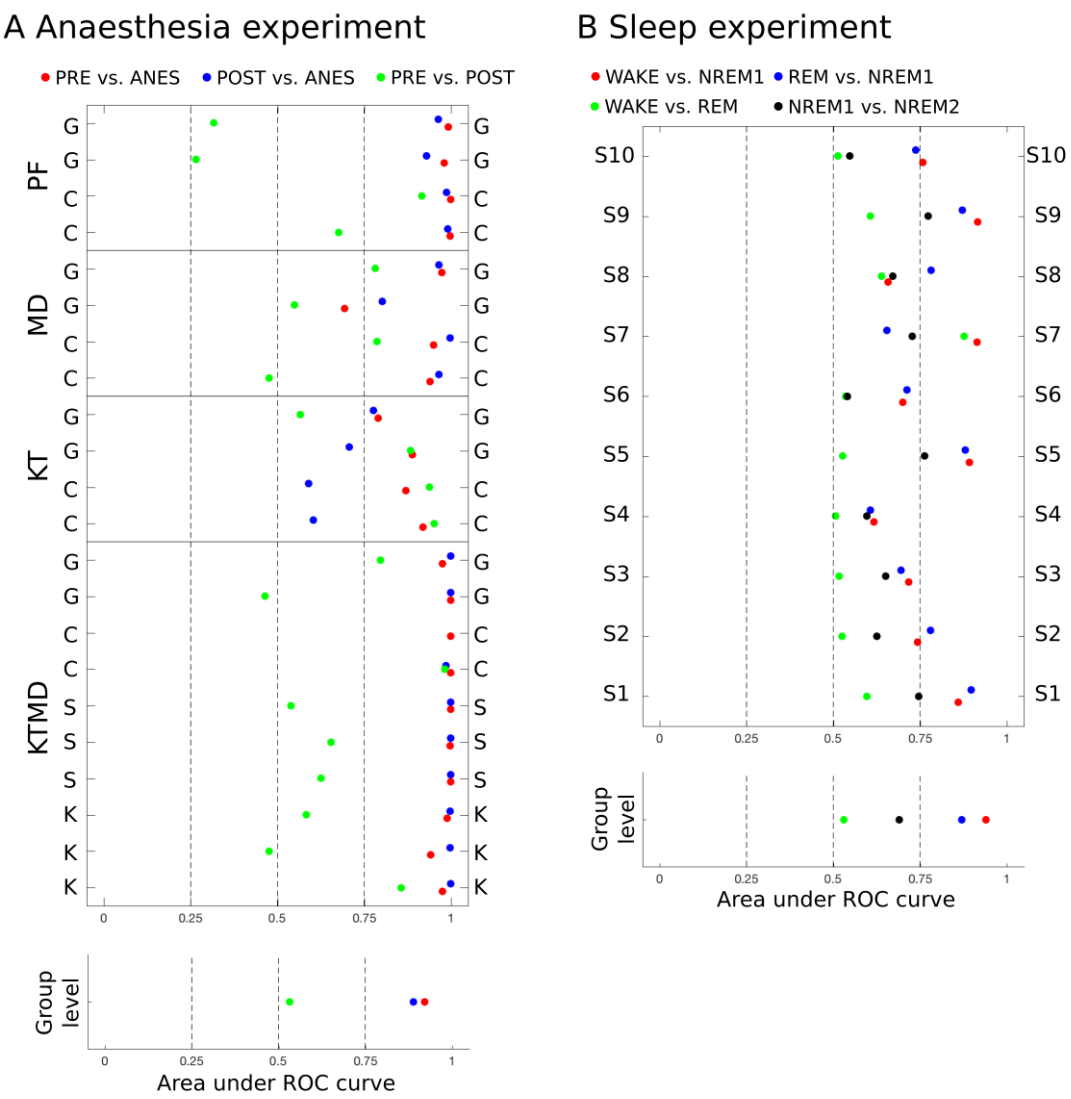
A Anaesthesia experiment
PRE vs. ANES
POST vs. ANES
PRE vs. POST
PF
MD
KT
KTMD
G
C
S
K
0
0.25
0.5
0.75
1
Group level
Area under ROC curve
B Sleep experiment
WAKE vs. NREM1
REM vs. NREM1
WAKE vs. REM
NREM1 vs. NREM2
S10
S9
S8
S7
S6
S5
S4
S3
S2
S1
Group level
Area under ROC curve

992 **Table 1.** Experimental sessions conducted in the macaque anesthesia study

| Monkey | Nr. | Code | Experiment date | Anesthetic agent (mg/kg) | Notes |
|---|---|---|---|---|---|
| Kin2 (K) | 1 | K-1 | 2011.05.13 | KT-MD (4.7; 0.019) | |
| | 2 | K-2 | 2011.05.25 | KT-MD (4.7; 0.019) | |
| | 3 | K-3 | 2011.05.24 | KT-MD (4.7; 0.019) | |
| Su (S) | 4 | S-1 | 2011.05.23 | KT-MD (8.8; 0.053) | |
| | 5 | S-2 | 2011.05.27 | KT-MD (8.8; 0.053) | |
| | 6 | S-3 | 2011.05.26 | KT-MD (8.8; 0.053) | |
| Chibi (C) | 7 | C-1 | 2011.06.22 | KT-MD (4.7; 0.019) | |
| | 8 | C-2 | 2011.06.21 | KT-MD (4.7; 0.019) | Missing *Post* data |
| | 9 | C-3 | 2012.08.09 | MD (0.017) | |
| | 10 | C-4 | 2012.07.20 | MD (0.017) | |
| | 11 | C-5 | 2012.08.13 | KT (4.3) | |
| | 12 | C-6 | 2012.07.19 | KT (4.3) | |
| | 13 | C-7 | 2012.08.02 | PF (5.2) | |
| | 14 | C-8 | 2012.07.30 | PF (5.2) | |
| George (G) | 15 | G-1 | 2011.01.12 | KT-MD (5.6; 0.011) | |
| | 16 | G-2 | 2011.01.13 | KT-MD (5.6; 0.011) | |
| | 17 | G-3 | 2012.08.14 | MD (0.019) | |
| | 18 | G-4 | 2012.07.26 | MD (0.019) | |
| | 19 | G-5 | 2012.07.24 | KT (5.9) | |
| | 20 | G-6 | 2012.08.10 | KT (5.9) | |
| | 21 | G-7 | 2012.08.03 | PF (5) | |
| | 22 | G-8 | 2012.07.31 | PF (5) | |

993

# Supplementary Materials

## Loss of consciousness is related to hyper-correlated gamma-band activity in anesthetized macaques and sleeping humans

**Michał Bola[1], Adam B Barrett[2], Andrea Pigorini[3], Lino Nobili[4], Anil K. Seth[2], Artur Marchewka[1]**

1: Laboratory of Brain Imaging, Neurobiology Center, Nencki Institute of Experimental Biology of Polish Academy of Sciences, Warsaw, Poland

2: Sackler Centre for Consciousness Science, Department of Informatics, University of Sussex, Brighton BN1 9QJ, UK

3: Department of Clinical Sciences, University of Milan, Milan 20157, Italy

4: Centre of Epilepsy Surgery "C. Munari", Niguarda Hospital, Milan, 20162, Italy

**Corresponding author:**
Michał Bola, PhD
Laboratory of Brain Imaging, Neurobiology Center
Nencki Institute of Experimental Biology
Polish Academy of Sciences
3 Pasteura Str., 02-093 Warsaw, Poland
Email: m.bola@nencki.gov.pl

# Supplementary results and discussion

## Control analyses

We conducted two additional analyses on the macaque anesthesia data-set to further support our findings. First, we show that reported effects can be found irrespective of the sliding window length, i.e. not only when using the 5 s long window (as in the main analysis), but also with shorter (3 s) and longer (10, 30, 60 s) windows (**Fig. S6**). Second, when comparing temporal covariation of signals between conditions the potential differences might, at least partially, stem from differences in amplitude and spectral content of the signals. Thus, we created surrogate data by shuffling the temporal order of windows within conditions (see: Methods section). However, *coupling strength* in the surrogate data was close to zero and thus surrogate-corrected results did not differ from the original results (**Fig. S6**). This indicates robustness of *coupling strength* to changes in amplitude of signals. Therefore, between-conditions differences in *coupling strength* do not stem directly from the differences in spectral profiles of signals, but rather from changes in the spatio-temporal coordination of activity.

## Analysis of other frequency bands

In the present study we investigated gamma-band oscillations (30-45Hz) in different states of consciousness. We focused on the gamma-band for the following reasons:

First, previous studies indicate that gamma-band activity is reliably correlated with neuronal firing rate (Whittingstall and Logothetis, 2009; Le Van Quyen et al., 2016) and thus changes in gamma might be interpreted as reflecting changes in spiking activity during loss of consciousness. At the same time (and likely for the same reason) amplitude of gamma-band oscillations is correlated with fMRI BOLD signal amplitude (Logothetis et al., 2001; Niessing et al., 2005), therefore studying gamma might provide physiological basis for effects previously observed using fMRI. Finally, changes in the gamma-band might be more directly related to existing theories of cortical processing, as gamma oscillations are hypothesized to constitute a basic computational process implemented in the brain (e.g. Fries et al., 2007).

Second, additional analyses of other frequency bands suggest that gamma-band coupling is the most promising correlate of LOC. Specifically we analyzed power (amplitude) and coupling strength for delta (1-4Hz), theta (4-8Hz), alpha (8-14Hz), and beta (20-30Hz) bands. Results of between-conditions post-hoc comparisons, which were conducted when ANOVA or the Friedman test indicated a significant effect of a state, are presented in **Fig. S7** (macaque anesthesia data) and in **Fig. S8** (human sleep data). To briefly summarize, in line with many previous studies we found a robust increase of delta power during anesthesia and NREM sleep. Further, analyzing co-activation

patterns in the macaque anesthesia data we found that increase in *coupling strength* in theta, alpha, and beta bands was also related to loss of consciousness. But changes in these bands were not replicated when analyzing the sleep data. Therefore, the between data-sets consistency suggests that the delta-band power and gamma-band amplitude-coupling constitute most robust correlates of consciousness and these changes are most likely to be replicated by future experiments.

Third, as pointed out above, in the macaque anesthesia dataset *coupling strength* increased during anesthesia in lower (theta, alpha) and higher (beta, gamma) frequency bands. But when investigating anesthetics-specific effects (**Fig. S9**) we noticed that a reliable association between an anesthetic used and a magnitude of a change can be found only in higher bands. The theta-band also exhibits robust increase in correlations during sedation but: i) there is high variability between subjects concerning the magnitude of the increase and, ii) the change is not correlated with the type of anesthetic agent used. Therefore, higher frequencies might better reflect different mechanism of action of various anesthetics.

# Supplementary figures

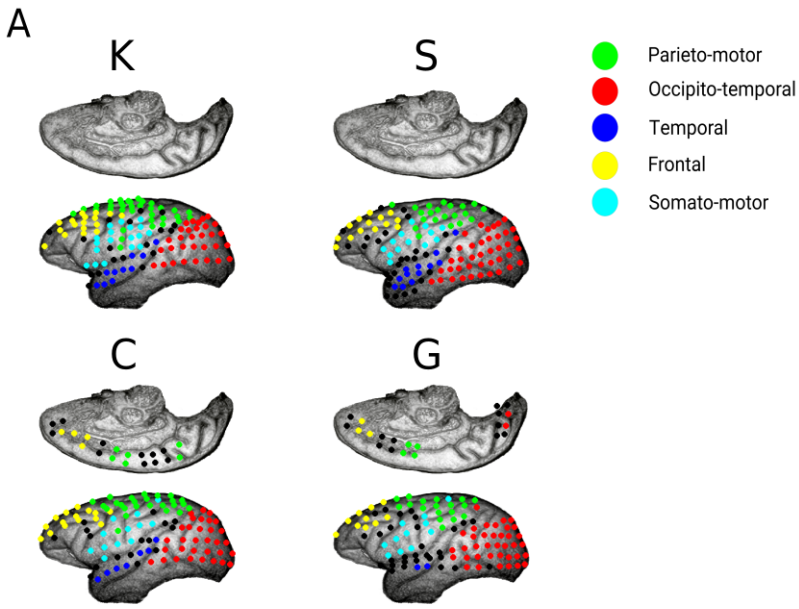


**Figure S1**. Electrode locations and anatomical modules in the anesthesia study. (**A**) Locations of electrodes for four monkeys tested in the anesthesia study. Colors indicate assignments of electrodes to the five anatomical modules detected by Goulas et al. (2014). Electrodes not assigned to any module are plotted in black.

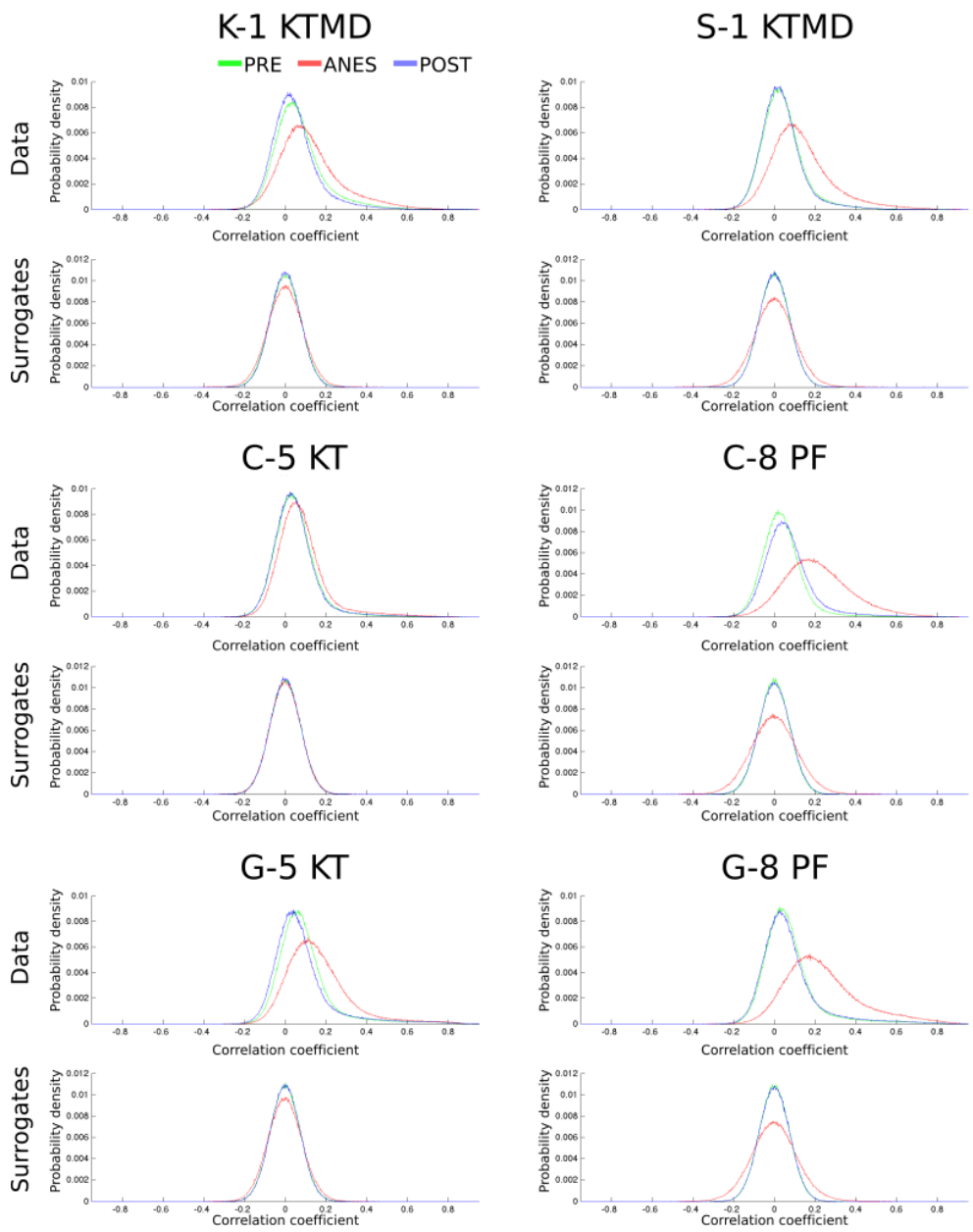


**Figure S2**. Anesthesia data-set histograms. Histograms indicate probability of observing a given correlation coefficient value within a full temporal correlation matrix (i.e. over all pairs of channels and all time-points). Both original data (upper panels) and surrogate data (lower panels) from six representative sessions are plotted.

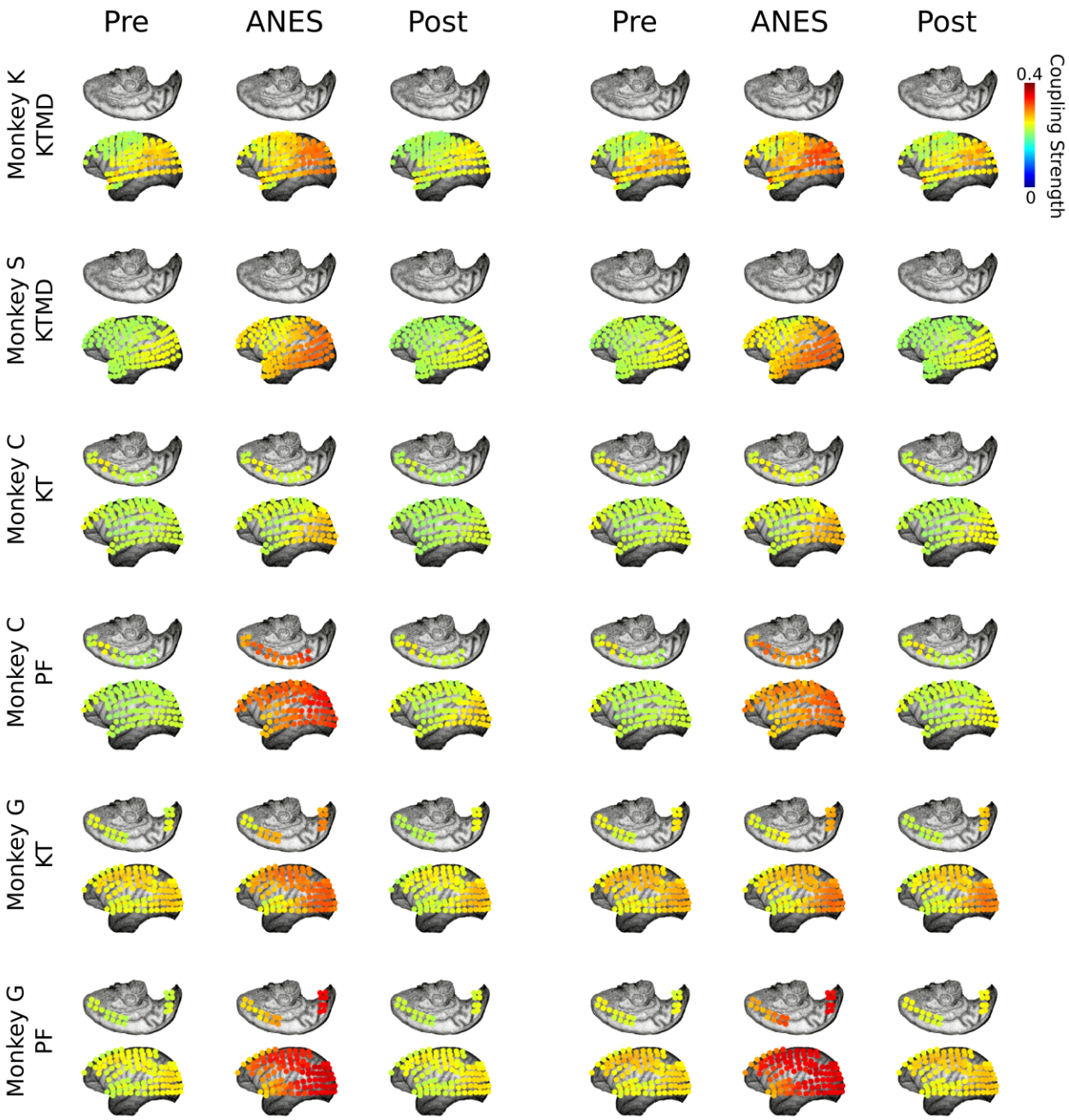


**Figure S3**. Nodal gamma-band *coupling strength* plotted for three conditions for 12 (out of 22) representative sessions.

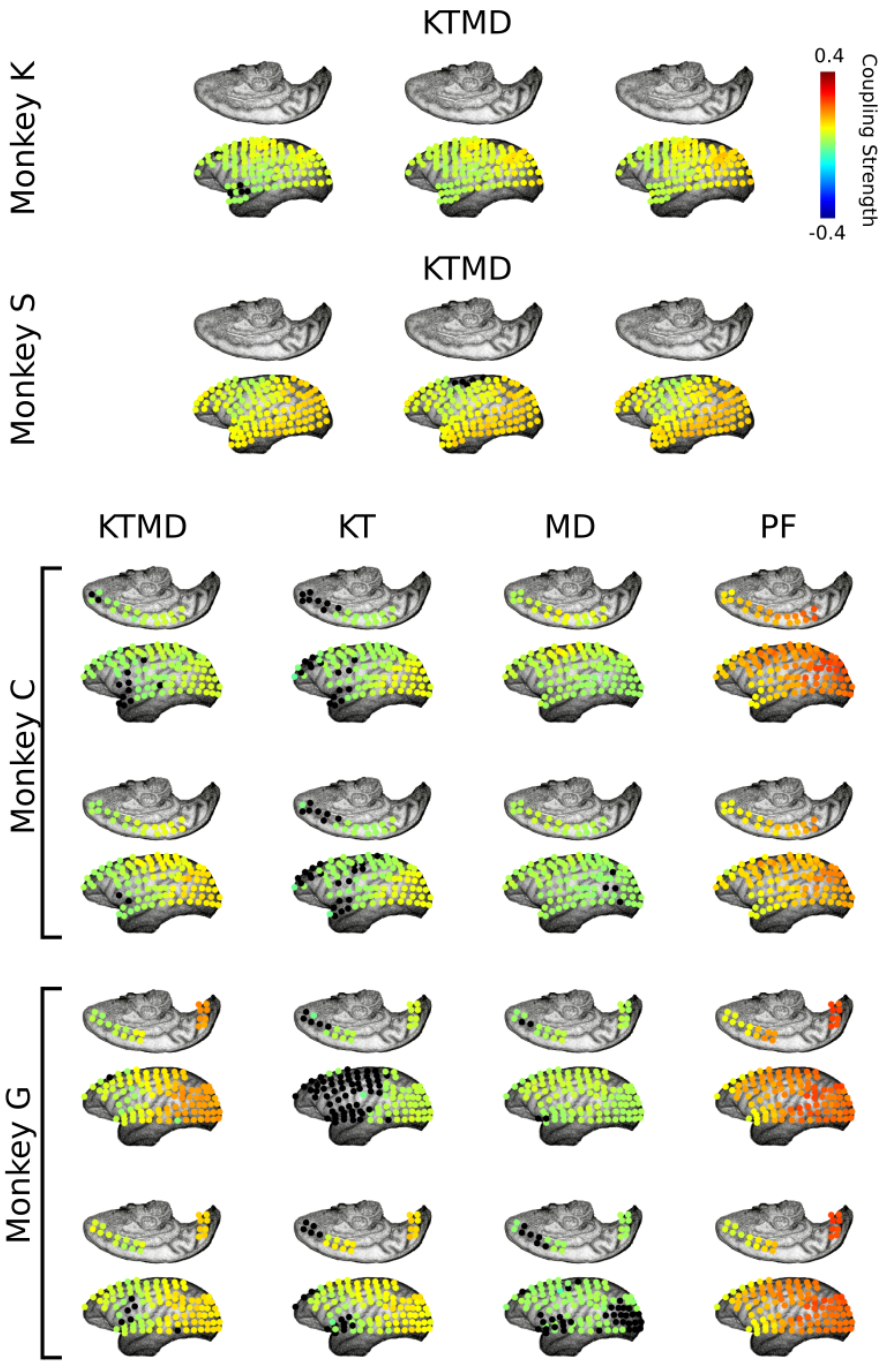


**Figure S4**. Anesthesia-related changes in gamma-band *coupling strength* over pre-anesthesia baseline (i.e. ANES – PRE). Each map presents results from one experimental session. Electrodes in color exhibited a significant change over pre-anesthesia baseline ($p<0.05$, Bonferroni corrected within each session), whereas electrodes in black did not exhibit a significant change. The maps of monkeys C and G are the same as in Fig. 5, but here they are not normalized.

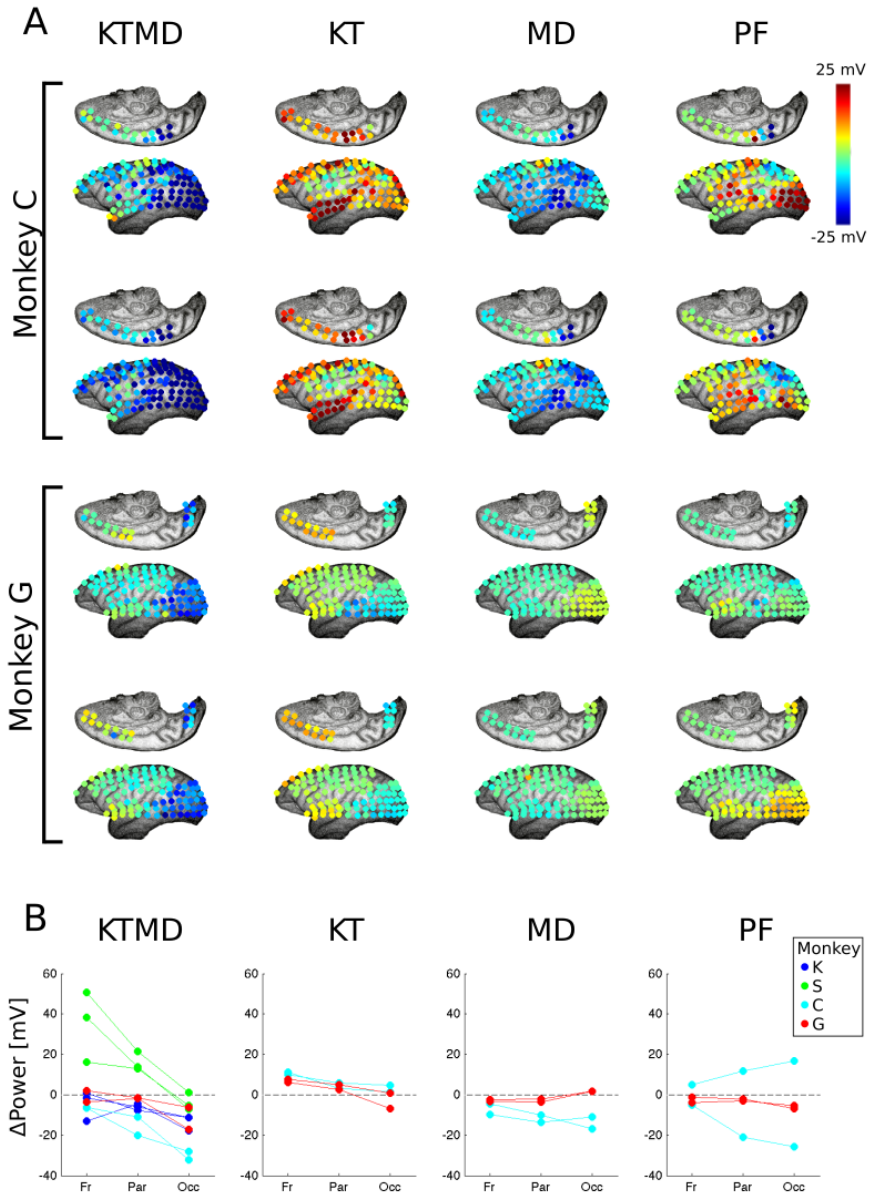


**Figure S5.** Anesthetics-specific topographic effects on gamma-band power. Compare to Fig. 5.

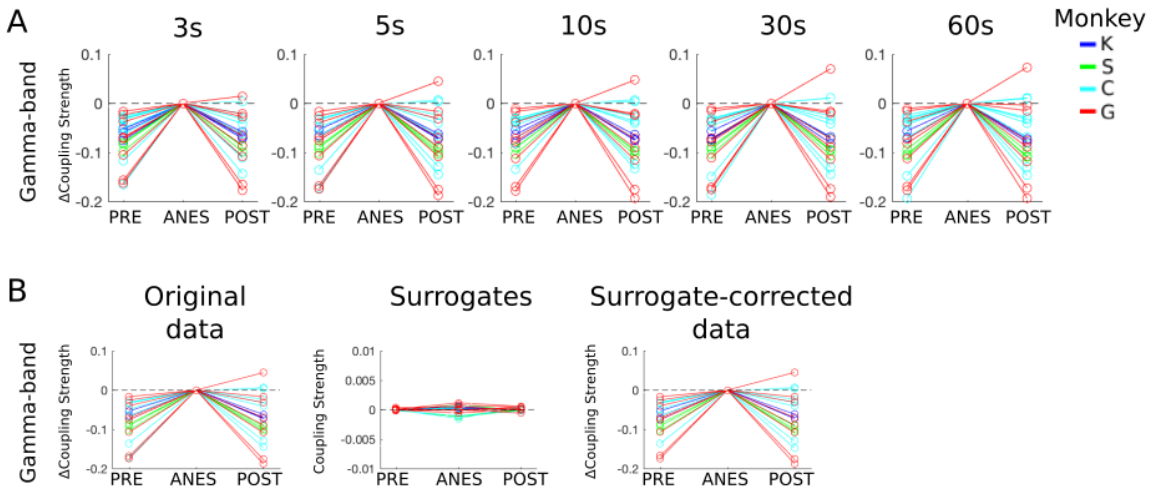


**Figure S6**. Control analyses conducted in the anesthesia data-set. Each triplet of data-points joined by a line represents one experimental session and colors indicate monkeys (as in Fig. 3). To facilitate comparison of anesthesia-induced effect results from each session are normalized by subtracting the ANES values (i.e. presented as *Δcoupling strength*). The data are visualized but not compared statistically. In **A** results obtained with different lengths of the sliding-window are plotted. Results obtained with the 5s-long window are the same as those presented in Fig. 3. In **B** surrogate-corrected results are presented. The original data presented in the left column are the same as those presented in Fig. 3. Surrogate corrected results were estimated by subtracting the value obtained from the surrogates from the original value (for each session and condition).

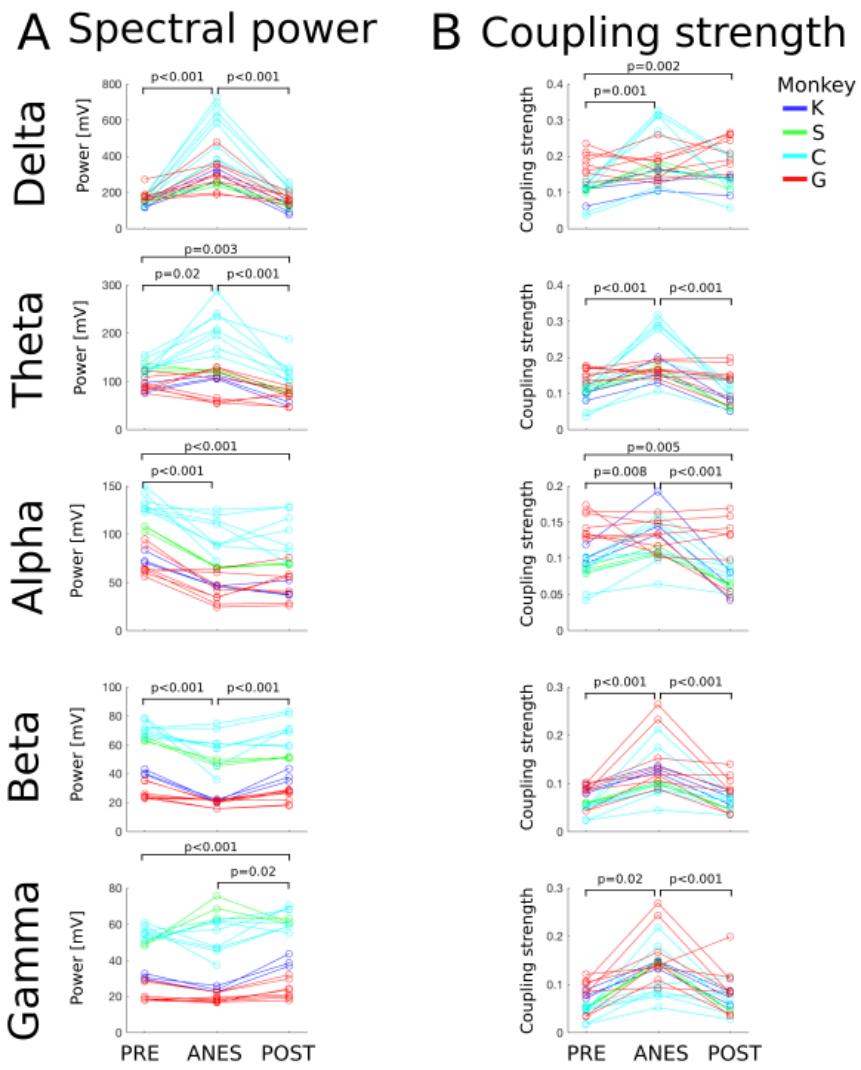


**Figure S7.** Power and *coupling strength* during wakefulness and anesthesia across all frequency bands – data from macaque monkeys.

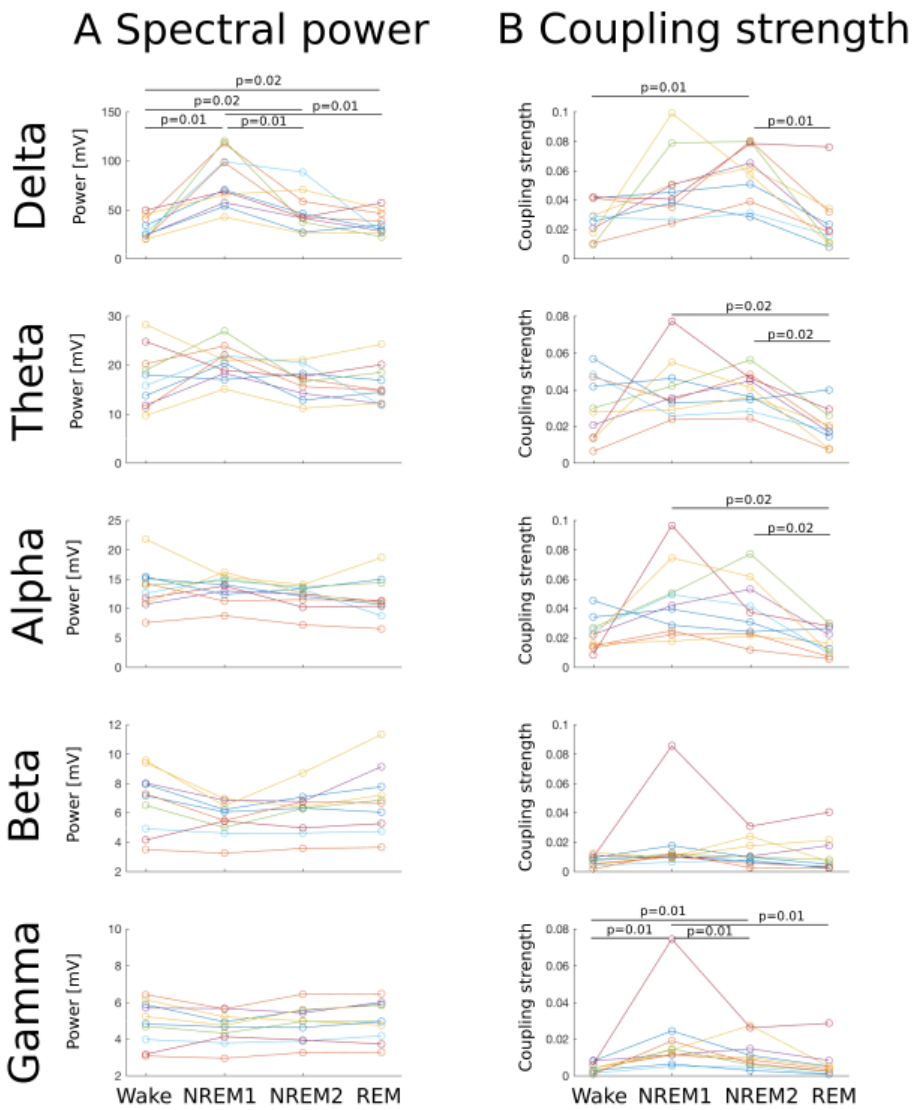


**Figure S8**. Power and *coupling strength* during wakefulness and anesthesia across all frequency bands – data from human subjects.

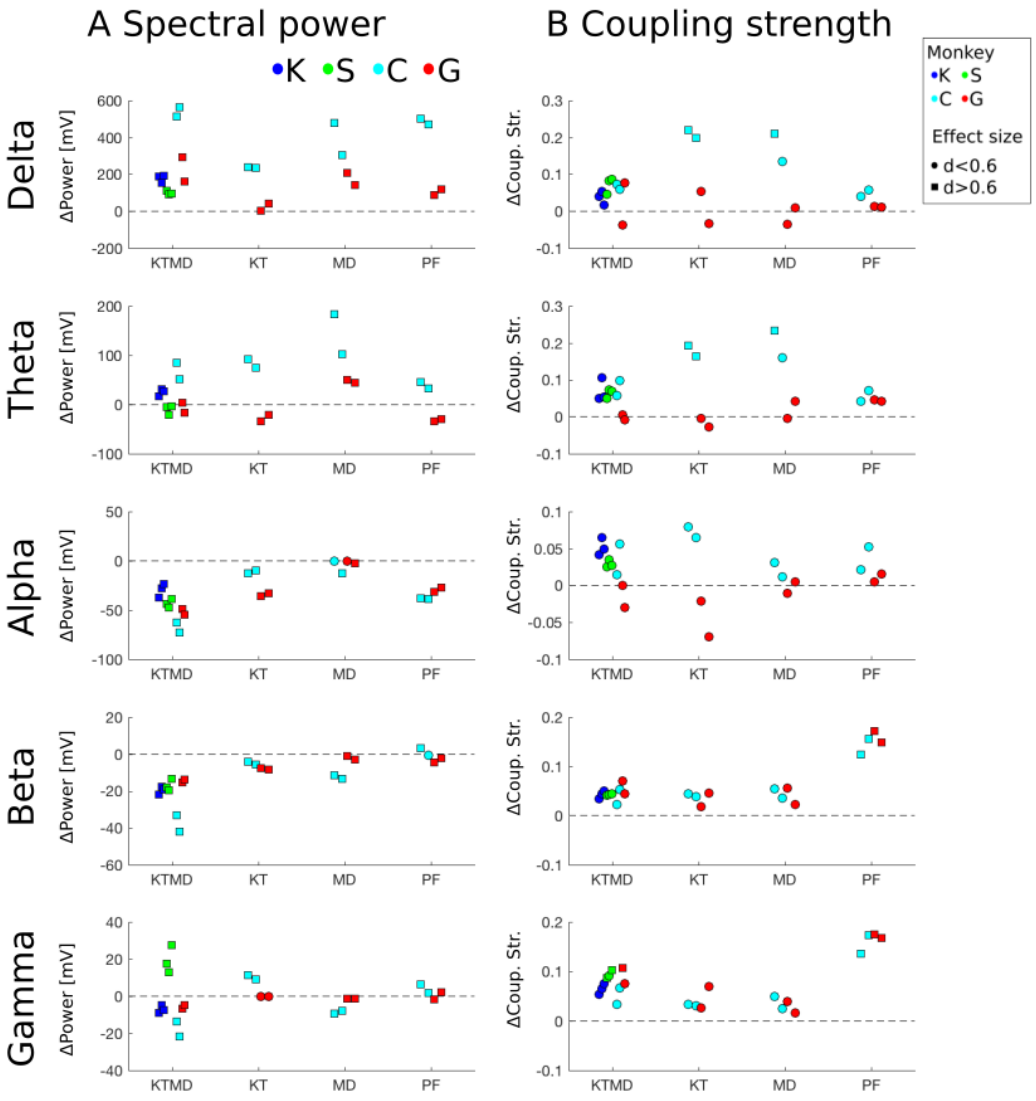


**Figure S9.** Anesthetics-specific effects on power and coupling strength in all frequency bands. Results presented in the same convention as in Fig. 4.